




Enhancing unmanned aerial vehicles logistics for dynamic delivery: a hybrid non-dominated sorting genetic algorithm II with Bayesian belief networks

Armin Mahmoodi¹ · Seyed Mojtaba Sajadi²  · Abdellatif M. Sadeq³ · Masoud Narenji⁴ · Mehdi Eshaghi¹ · Milad Jasemi⁵

Received: 12 May 2024 / Accepted: 21 January 2025
© The Author(s) 2025

Abstract

To address the complexities of managing networks of unmanned aerial vehicles (UAVs) and Just-in-Time problem solving, this study introduces a cutting-edge multi-objective location-routing optimization model. This model integrates time window constraints, concurrent pick-up and delivery demands, and rechargeable battery functionality, significantly enhancing the efficiency of UAV operations. It reduces battery consumption and transportation costs while optimizing delivery times and reducing operational risks. The model improves the refinement of delivery schedules by accounting for uncertain traffic scenarios, thereby increasing its accuracy and reliability in dynamic environments. Additionally, a Bayesian belief networks approach for risk assessment introduces a new layer to operational risk management. The model's performance and its trade-offs are demonstrated through advanced data visualizations such as 3D Pareto fronts, pair plots, and network graphs, with validation via the NSGA-II approach confirming its reliability and practical applicability. This research represents a major leap forward in drone routing strategies, focusing on efficiency, adaptability, and risk management in UAV logistics and provides a comprehensive framework that bridges the gap between theoretical exploration and practical application.

Keywords Routing problem · Drone delivery · NSGA-II algorithm · Multi-objective optimization · Bayesian belief networks · Risk assessment

1 Introduction

Unmanned aerial vehicles (UAV) are one of the most intensively studied technologies in logistics in recent years (Mulumba & Diabat, 2024; Chung et al., 2020; Li et al., 2021; Mahmoodi et al., 2024). In this system, as a UAV delivers logistics services to customers, it can also concurrently serve nearby customers. This collaborative delivery system enhances the overall efficiency of logistics operations (Bi et al., 2024; Luo et al., 2021a, 2021b; Murray & Chu, 2015). In contrast to other vehicles, UAVs offer several advantages, including lower capital and operating costs, the ability to take off and land in confined spaces without the need for costly infrastructure, and the elimination of the requirement for an onboard operator. These advantages make UAVs highly beneficial for various transportation and logistics activities

Extended author information available on the last page of the article

(Wei et al., 2021). Numerous industrial companies, including Amazon, FedEx and DHL are actively vying to pioneer the implementation of UAV delivery systems (Wang et al., 2024). These companies integrate technological features aligned with current trends in the transportation industry and society, such as autonomy, flexibility, and agility. The primary goal of UAV deployment is to reduce overall costs and enhance customer satisfaction through swift last-mile deliveries. The efficiency of last-mile operations not only impacts the profitability of retailing but also influences environmental and social performance criteria, including emissions and traffic congestion in various regions. The adoption of UAVs in delivery processes has a substantial effect on energy consumption and contributes to the reduction of pollution, including greenhouse gas emissions and carbon footprint (Chi et al., 2023; Sham et al., 2023).

While the developed UAV system offers advantages, challenges arise in real-time processes, including unexpected weather, safety, security of data, limited capacity, and budget of purchasing equipment and infrastructure. These challenges become more prominent when UAVs need to predict cases and choose optimal routes. However, ongoing development and testing may soon enable UAVs to deliver packages using AI technology. This encompasses tasks like launch, navigation, data acquisition, transmission, and analysis. An accurately designed AI optimization model ensures feasible and efficient operating decisions for UAV delivery systems (Eskandaripour & Boldsaiikhan, 2023; Yu et al., 2022).

In mission platform design models, the comprehensiveness of objectives correlates with real-world applicability, enabling the model to generate pragmatic solutions. Key objectives explored in these cases involve minimizing travel time, reducing energy consumption, maximizing reliability, and lowering operational costs (Kumbhar & Shin, 2022; Wei et al., 2021).

In this research to enhance the UAV delivery system, we create a comprehensive multi-objective optimization model. The aim was to devise an advanced transportation scheme addressing four pivotal objectives: Minimizing operational cost, reliable delivery time estimation, imposed risk, and battery consumption. These factors were identified as crucial for optimizing the delivery system. The optimization is represented through an integrated mixed-integer non-linear program (MINLP) problem in the objective function, framing the decision problem to determine the optimal location and routing for a fleet of UAVs (Yakıcı & Karatas, 2021). In this scenario, there is a set of demand points, UAV fleets, and candidate distribution centers (DCs) considered. While not all demand points need to be visited, each visited point yields a specific benefit. The primary objective is to maximize the overall operational benefit obtained by visiting these points. The simultaneous execution involves selecting allowed stations, assigning UAVs to these stations, and assigning UAVs to DCs. Additionally, the authors address an extension of this problem, allowing demand points to have time windows for UAV visits and enabling UAV takeoff and landing at assigned DCs and different demand points. The model focuses on location, routing, and prize (benefit) collection, contributing significant advancements to each aspect of the optimization goals (Sham et al., 2023). Below the contributions featured in this article:

This paper makes significant strides in UAV logistics through a series of interconnected contributions, starting with its sophisticated mathematical formulation that tackles the UAVs' location-routing problem with dual objectives of minimizing operational costs and maximizing customer satisfaction, as innovatively proposed by Ning and You (2019). It further introduces a nuanced battery consumption model, highlighted by Torabbeigi et al. (2020), which smartly integrates the payload's effect on battery life into the operational planning, balancing efficiency with cost-effectiveness. The inclusion of a risk assessment model, as explored by Jiao et al. (2022), introduces a fourth objective function using Bayesian belief networks to proactively manage the operational risks associated with increasing UAV

usage, enhancing system reliability and airspace security. Lastly, the application of a genetic algorithm validates the model's effectiveness, demonstrating UAVs as a time-saving and environmentally friendly alternative for package delivery. Collectively, these contributions not only advance the academic discourse on UAV logistics but also provide tangible, practical solutions for real-world challenges in the delivery sector, setting new standards for efficiency, reliability, and sustainability (Yang et al., 2023).

The remaining sections of our paper are organized as follows. In Sect. 2, we provide an overview of existing models related to the UAV routing problem, highlighting their distinctive features. Section 3 is dedicated to elucidating the formulation of our model and detailing its components. Moving on to Sect. 4, solutions are presented, addressing various aspects of the model through the application of a reinforcement algorithm. In Sect. 5, numerical results are presented, followed by Sect. 6, which provides a comparative analysis and validation of the optimization results. Finally, Sect. 7 concludes the paper, offering a summary of the entire research structure.

2 Literature review

Optimizing UAV routing has become a focal point for researchers in recent times. Numerous research teams have undertaken thorough examinations of contemporary studies related to UAV delivery and operations. Notably, Rojas et al. (2021) and Marcina et al. (2020) have conducted reviews focusing on generic UAV routing issues and parcel delivery, respectively. The common thread in these studies is the assumption that minimizing delivery completion time or costs constitutes a primary optimization objective for UAV delivery models. The landscape of modern transportation is rapidly evolving, posing a complex challenge for conventional routing methods originally designed for traditional vehicles. Nonetheless, there is a promising subset of solutions embracing a rigorous analytical approach. These solutions employ mathematical calculations to discern optimal routes while simultaneously addressing multiple objectives (Kumbhar & Shin, 2022).

2.1 UAV routing problem utilizing a multi-objective hybrid optimization framework

The literature on UAV-based product delivery has seen numerous studies, significantly contributing to the advancement of routing and location problems associated with distribution centers (DCs) (Wang et al., 2024). Some studies have introduced innovative routing models, proposing operations that involve both UAVs and trucks. In a recent investigation, Bhuiyan et al. (2022) delved into the optimization of UAV deployment for direct goods delivery within specified time windows. They presented a multi-objective model, employing a novel mathematical optimization-based decision-making approach. This model assists business owners in optimally routing their UAV fleets by minimizing total energy consumption, required fleet size, and the number of additional batteries needed. In addition to them, Hashemi et al., (2021, 2022) in another research focused on location and routing problems within the supply chain, involving manufacturers, distributor candidate sites, and retailers. The objective is to minimize delivery times and system costs for retailers, with a focus on determining optimal routing and distributor locations. The study employs unique criteria, considering factors such as simultaneous deliveries and pickups, soft and hard time windows for retail services, and various costs including transportation, distributor construction, vehicle acquisition, and manufacturing. The conceptual model is developed and modeled, and solutions are explored

using General Algebraic Modeling System software (GAMS), as well as Multiple Objective Particle Swarm Optimization (MOPSO) and non-dominated sorting genetic algorithm II (NSGAI) algorithms in small dimensions (Freitas et al., 2022).

Another noteworthy contribution comes from Mahmoodi et al., who pioneered a combined parcel delivery routing problem with the aim of minimizing total delivery time, cost, and time. Their model incorporates realistic features of UAV delivery networks, considering routing limitations, costs, various distance metrics for UAVs, and risk assessment based on the Specific Operations Risk Assessment (SORA) standard. This study proposes a multi-objective location-routing optimization model that addresses time window constraints, simultaneous pick-up and delivery demands, and the potential for recharging used batteries. The objectives include reducing transport costs, delivery times, and estimated risks. The optimization of delivery time also accounts for uncertain conditions in potential traffic scenarios. Risk assessment follows the SORA standard, aligning with the approach of previous studies (Zhang et al., 2022).

They present a groundbreaking approach to enhance UAV logistics through a sophisticated multi-objective hybrid optimization model. The framework is meticulously crafted, drawing inspiration from the SORA standards, to elevate the performance of advanced delivery systems. They made a noteworthy contribution by addressing a combined parcel delivery routing problem, minimizing total delivery time, cost, and time. Their model incorporates realistic features of UAV delivery networks, considering routing limitations, costs, various distance metrics for UAVs, and risk assessment based on the Specific Operations Risk Assessment (SORA) standard. This study proposes a multi-objective location-routing optimization model, addressing time window constraints, simultaneous pick-up and delivery demands, and the potential for recharging used batteries, with objectives encompassing reduced transport costs, delivery times, and estimated risks (Mahmoodi et al., 2022).

Millar et al. (2023) introduced a novel concept involving the coordinated operation of multiple Unmanned Aerial Vehicles (UAVs) under the guidance of a manned "Tender" air vehicle equipped with a pilot and flight manager(s). The paper also addresses trajectory optimization for UAVs tasked with collecting data from sensors in a continuous space. The path-planning problem is formulated for a cooperative swarm of UAVs, aiming to maximize data accumulation within flight time constraints and minimize potential risks. Risk assessment is conducted using a Specific Operation Risk Assessment—Bayesian belief network approach, and the resulting analysis is weighted through an analytic hierarchy process ranking model. The proposed network architecture demonstrates the capability of UAVs to make optimal movement decisions while addressing various objectives (Sajid et al., 2022).

An UAV-based routing problem with multiple objectives, including minimizing distance traveled, increasing customer satisfaction, and reducing the number of used UAV has been tackled (Macrina et al., 2020). Their study resulted in obtaining the Pareto Front (Janik et al., 2021; Nguyen et al., 2023). In a different approach, adapted a strategy from the traveling salesman location routing problem to determine the UAV's shortest route. They utilized the ant algorithm to identify the optimal route and select an ideal location for DCs (Chauhan et al., 2020).

2.2 Cost-integrated UAV routing problem

We improve upon the multi-routing delivery problem by incorporating pick-up services. Specifically, our focus involves three categories of customers: those requiring delivery, pick-up, and simultaneous delivery & pick-up services. In this context, a truck, in conjunction

with multiple UAVs, caters to all customer needs. A UAV, upon completing a delivery service, can redirect to a customer requiring pick-up service rather than returning directly to the truck or depot. This approach maximizes UAV capacity utilization, ensuring diverse customer demands are met efficiently. Unlike prior studies that predominantly optimize either transportation costs (Liu et al., 2021; Luo et al., 2021a, 2021b; Mahmoodi & Hashemi, 2024; Ha et al., 2018) or delivery time (Murray & Chu, 2015; Dell'Amico et al., 2022; Vu et al., 2022), our consideration encompasses broader aspects of logistics activities crucial for a logistics company. For instance, non-emergency logistics services may have soft time windows, necessitating vehicles to complete services within an optimal time range, referred to as service reliability. Given that the initial arriving vehicle at a rendezvous may need to wait for others, minimizing waiting time becomes pivotal. Therefore, we introduce a multi-objective truck-UAV collaborative routing problem incorporating delivery and pick-up services (MCRP-DP). This model simultaneously accounts for transportation costs, service reliability, and vehicle waiting time.

Furthermore, several studies have implemented multi-objective optimization in truck-UAV collaborative delivery systems. Wang et al. (2020) proposed a bi-objective version of the FSTSP and an improved NSGA-II algorithm to address the problem. In a similar vein, Das et al. (2020) implemented collaborative Pareto ant colony optimization to optimize transportation costs and customer service levels, specifically focusing on timely deliveries in a synchronized truck and UAV delivery system.

2.3 UAV routing problem with risk assessment incorporating bayesian belief networks

The incorporation of IoT devices during data transmission increases the susceptibility of UAVs to security risks and safety hazards (Balador et al., 2018). Recent advances in state-space models (SSMs) and Gaussian graphical models have significantly contributed to constructing Bayesian belief networks for biological systems. Dynamic state space models with hierarchical Bayesian settings have been developed to infer genetic networks and dynamic profiles associated with disease treatments, effectively capturing genomic changes and gene–gene interactions over time using Monte Carlo Markov Chain and Gibbs sampling algorithms (Liang & Kelemen, 2016; Roweis & Ghahramani, 1999). Additionally, GraphEM, a method for estimating transition matrices in linear-Gaussian SSMs by relating them to adjacency matrices of directed graphs, has demonstrated good performance and interpretability in uncovering causal relationships (Elvira & Chouzenoux, 2022). Converting Markov chains and hidden Markov models into Gaussian processes has provided the advantage of continuous time scale support and flexible covariance function modification, addressing limitations of discrete time scales and linear conditional relationships (Chouzenoux & Elvira, 2024). Furthermore, LaGrangEM estimates parameters in non-Markovian linear-Gaussian latent processes by incorporating prior knowledge through a graphical interpretation, connecting with Granger causality and offering superior performance in estimating causal relationships and delays (Nagakura, 2019). These methodologies enhance the robustness and applicability of Bayesian belief networks in precision medicine and personalized healthcare. Various measures have been employed by researchers to analyze the operational risks of UAVs. Millar et al., introduced the Bayesian belief network (BBN) for interim flight clearances, using this method to identify key elements contributing to risks and dangers in experimental Unmanned Aircraft Systems (UAS) flight tests (Millar, 2015). In another study (Millar et al., 2023), examined several research questions in their study. Firstly, they sought to assess the

feasibility and potential of operating multiple UAVs commanded and supported by a manned 'Tender' air vehicle. Secondly, they aimed to find the optimal trajectories for UAVs to collect data from sensors in a predefined continuous space. Lastly, they aimed to formulate the path-planning problem for a cooperative, diverse swarm of UAVs tasked with optimizing multiple objectives simultaneously. The key findings of the study indicate that the multi-objective reinforcement learning (MORL) architecture can successfully train each UAV to make optimal movement decisions based on network state observations. Additionally, the algorithm demonstrated decreasing errors in the learning process as the epoch number increased (Shen & Sun, 2023).

To enhance operational safety, researchers have devised autonomous mechanisms for prompt error response in UAV networks, as demonstrated in work by Allouch et al. (2019). Additionally, Kishk et al. developed a UAV-enabled cellular network using tethered UAVs (UAVs), making the UAV safer and more resilient to winds and adverse weather conditions through the tethered connection to a Ground Station (GS) (Kishk et al., 2020). In another study, Mahmoodi et al. estimate the imposed risks of selected trajectories using the SORA standard developed by the European Aviation Safety Agency (EASA). The study demonstrated that identified risks in each trajectory were modeled and minimized as the third objective. Notably, this research marked the first instance of risk assessment utilizing an AHP approach based on the SORA standard (Mahmoodi et al., 2022). In the same way (Janik et al., 2021; Hu et al., 2020; Baubion, 2013; Erkut & Ingolfsson, 2005; SORA Standard, 2021). Capitán et al. conducted a risk assessment for aerial shooting operations using the SORA method in their papers. The papers comprehensively explore all stages of the SORA, assesses operational risks, and proposes corrective actions to mitigate risks within the system. Moreover, Chang and Laliberte (2023) in a research study covers the optimization of trajectories for Unmanned Aerial vehicles (UAV), incorporating aspects such as solar energy systems, energy harvesting, wing planforms, dynamic soaring, and sensitivity analysis. The focus is likely on enhancing the efficiency and performance of UAV by optimizing their flight paths, considering renewable energy sources like solar power, and analyzing the sensitivity of the system to various parameters. The study may explore innovative wing designs and dynamic soaring techniques for improved trajectory planning and energy efficiency in Remotely Piloted Aircraft System (RPAS) (Nguyen et al., 2022).

2.4 UAV routing problem incorporating battery consumption considerations

The primary constraint in practical UAV-based deliveries is the limited battery energy capacity, which restricts the range of UAV delivery. In the context of drone deployment optimization for direct delivery with time windows and battery replacements, the most used theories include mathematical optimization-based decision-making methodology, which serves as the foundation for developing mathematical optimization models for drone fleet routing. The research methods commonly employed in this field are mixed-integer programming (MIP) models (Bhuiyan et al., 2022), which are utilized to formulate and solve the optimization with drone with drone and energy and energy consumption analysis. The authors (Bhuiyan et al., 2022) The study developed an optimization model for efficient drone fleet routing to minimize fleet size, battery needs, and energy consumption; investigated how business and drone operating conditions affect these metrics; and analyzed real flight and delivery data to understand the impact of operating parameters on energy consumption, fleet size, and battery replacement needs. The key findings of the study indicate that flying drones over road networks significantly increases total energy consumption, required fleet size, and the required number

of battery replacements compared to flying in a straight path. Additionally, using a mixed fleet of hexacopter and quadcopter drones reduces total energy consumption compared to using a homogeneous fleet of only hexacopters. The delivery range, energy consumption, and required fleet size are also affected by drone speed, package weight, flight path, and minimum required battery energy (Kyriakakis et al., 2023).

San et al. (2016) introduced a Genetic algorithm-based procedure for assigning UAVs to deliver packages to customer locations. Subsequently, Song et al. (2018) formulated the UAV delivery problem as a mixed-integer program, solved through a heuristic algorithm. Unlike previous works by Yadav and Narasimhamurthy (2017) and San et al. (2016), Song et al. considered the impact of package weight on UAV flight time, reflecting the limitations of battery capacity. However, other factors such as UAV speed and flight path were not incorporated into the energy consumption calculations, and there was no explicit modeling of battery energy consumption or replacements.

Dorling et al. (2017) addressed battery energy consumption by modeling it as a function of UAV battery and package weight. They proposed mixed-integer linear programming formulations for two variants of a UAV routing problem, with the objectives of minimizing total delivery time and total cost, respectively. The model assumes that each UAV can deliver multiple packages to different customers in a single trip, ensuring that the battery capacity is sufficient for a trip before it commences. However, this study does not explicitly model the minimum energy requirement for determining battery replacement, nor does it aim to minimize the number of battery replacements.

Rabta et al (2018) tackled a UAV routing problem along with decisions regarding UAV battery charging locations for delivering disaster relief packages, presented as a mixed-integer program. Like (Dorling et al., 2017), each UAV can deliver multiple packages in a single trip, and battery consumption is influenced by package weight. Their model tracks the remaining UAV battery energy using a variable in the model to determine the need for charging. However, the battery charging process was not explicitly modeled to account for charging time or rate.

2.5 UAV routing problem incorporating time constraints

Several studies have addressed the incorporation of time windows for customer deliveries in UAV routing problems, optimizing fleet size to enhance customer order fulfillment. A capacitated vehicle routing problem with time windows as a mixed-integer program to minimize the required number of UAVs and batteries has been formulated by Troudi (Troudi et al., 2018). Like (Dorling et al., 2017), the authors assumed multiple packages could be carried by each UAV in a single trip, with battery replacement after each trip. They aimed to minimize the number of batteries used by reducing the number of trips.

Cheng et al. (2020) delved into a multi-trip UAV routing problem with time windows, seeking to minimize travel and electricity consumption costs related to UAV batteries. They considered UAV energy consumption as a function of package weight and distance traveled, although they used theoretical power consumption during hovering, which may not be realistic. Kong et al. (2023) studied another multi-trip UAV delivery problem with time windows, aiming to minimize the total routing distance in delivering parcels to customers. Choi and Schonfeld (2017) focused on an automated UAV delivery system, optimizing fleet size to minimize the total cost. The authors showcased the sensitivity of UAV speed and battery capacity on the system cost and fleet size, respectively. All these studies assumed a homogeneous UAV fleet.

Coelho et al. (2017) expanded the scope to a mixed fleet of UAVs, aiming to minimize total distance, delivery time, and the number of UAVs used. However, they considered UAV energy consumption solely as a function of UAV speed. It's worth noting that all the mentioned studies assume each UAV delivers packages to multiple customers in a single trip, replacing the battery after each trip. This assumption, however, may not align with practical scenarios where UAVs are designed to carry a single package on a trip. Replacing the battery after each return can lead to unnecessary battery replacements and reduced UAV utilization (Bi et al., 2023).

In addition to these studies, some focused on the impact of UAV delivery on carbon emissions (Chiang et al., 2019; Figliozzi, 2017) as well as the location of UAV deployment and charging facilities to improve demand coverage (Chauhan et al., 2019; Trotta et al., 2018). Notably, only two variants of the UAV collaborative routing problem considered both delivery and pick-up services based on the SORA standard (Janik et al., 2021; Mahmoodi et al., 2022). However, these studies lacked synchronization in UAV service to customers, updated UAV capacity based on parcel weight, and overlooked customer residence details. The current study distinguishes itself by simultaneously optimizing four objectives using a novel evolutionary multi-objective algorithm, setting it apart from other investigations.

A thorough review of literature on multiple criteria in course scheduling issues was conducted using the Scopus database. The search terms included combinations of " Optimization Methods " or " Hybridization " with " Truck-Drone Delivery ", " Drone Delivery ". Since 1995, this search identified 71 relevant papers. However, exclusions were made for reasons such as duplication, and non-research content like editorial notes, leaving 30 papers that address multiple objective issues in course scheduling, as detailed in Table 1.

3 Problem description and formulation

In the rapidly evolving landscape of logistics and transportation, the integration of unmanned aerial vehicles (UAVs) or UAVs has emerged as a promising solution to address the challenges of last-mile delivery. The efficiency and speed of UAV deliveries have the potential to revolutionize the way goods are transported, offering swift and cost-effective alternatives to traditional delivery methods. However, to fully harness the benefits of UAV technology, it is crucial to develop sophisticated optimization strategies that consider real-world constraints.

This problem description revolves around the design and optimization of a UAV delivery system, considering the intricate interplay between distributor locations, facility hubs, customer demand points, and the unique challenges posed by recharging constraints. With a carefully defined set of parameters, including distributor candidate locations (D), facility locations (F), demand points (P), the fleet of UAVs (K), recharging-capable points (D1), non-recharging points (D2), and distinct scenarios (U), the task at hand is to create a system that maximizes operational efficiency while adhering to the constraints imposed by energy limitations.

3.1 Problem description

In the context of designing an efficient UAV delivery system, the objective is to optimize the delivery routes and UAV assignments for a given set of parameters. The system is characterized by the following assumptions:

Table 1 Comprehensive review of global academic databases addressing multiple objective course scheduling challenges

References	Optimization methods	Hybridization			Datasets			Objective functions			
		Truck-drone delivery	Drone delivery	benchmark	Real world	Reference point	Weight sum	Pareto dominance			
Bi et al. (2024)	Multi-Agent Reinforcement Learning	✓		✓							✓
Mulumba and Diabat (2024)	Metaheuristic Optimization Algorithms		✓	✓	✓						✓
Eskandaripour and Boldsakhan (2023)	Metaheuristic Optimization Algorithms	✓	✓	✓					✓		✓
Kumbhar and Shin (2022)	Machine Learning	✓		✓					✓		✓
Arishi et al. (2022)	Machine Learning	✓		✓					✓		✓
Guo et al. (2023)	Reinforcement Learning		✓		✓						✓
Jiao et al. (2023)	Dynamic Model	✓	✓	✓						✓	
Kyriakakis et al. (2023)	GRASP/VND algorithm	✓	✓	✓	✓						✓
Sham et al. (2023)	Metaheuristic Optimization Algorithms	✓	✓	✓	✓						✓
Bhuiyan et al. (2022)	Metaheuristic Optimization Algorithms	✓	✓	✓	✓						✓
Hashemi et al (2022)	Meta-Heuristic Algorithms		✓	✓							✓
Nguyen et al (2022)	Meta-Heuristic Algorithms	✓		✓					✓		✓
Mahmoodi et al. (2022)	Robust Optimization Model		✓	✓							✓
Millar et al. (2023)	Reinforcement Learning Algorithm		✓	✓							✓
Dell'Amico et al. (2022)	Meta-Heuristic Algorithms		✓	✓							✓
Vu et al. (2022)	Meta-Heuristic Algorithms	✓		✓	✓						✓
Liu et al. (2022)	Reinforcement Learning		✓	✓	✓						✓
Gohari et al. (2022)	Meta-Heuristic Algorithms		✓	✓							✓
Chang and Laliberte (2023)	Meta-Heuristic Algorithms		✓	✓							✓
Wu et al. (2022)	Meta-Heuristic Algorithms	✓		✓							✓
Kong et al. (2023)	Meta-Heuristic Algorithms		✓	✓							✓
Nguyen et al. (2022)	Meta-Heuristic Algorithms		✓	✓							✓
Shen and Sun (2023)	Metaheuristic Optimization Algorithms		✓	✓							✓
Zhang et al. (2022)	Machine Learning	✓		✓							✓
Yu et al. (2022)	Meta-Heuristic Algorithms	✓		✓							✓

Table 1 (continued)

References	Optimization methods	Hybridization		Datasets		Objective functions		
		Truck-drone delivery	Drone delivery	benchmark	Real world	Reference point	Weight sum	Pareto dominance
Yang et al. (2023)	Multi-Agent Reinforcement Learning	✓	✓	✓				✓
Freitas et al. (2022)	Exact And Heuristic Approaches	✓		✓				✓
Sajid et al. (2022)	Metaheuristic Optimization Algorithms	✓		✓				✓
Bi et al. (2023)	Deep Reinforcement Learning	✓		✓				✓
Our Article	Meta-Heuristic Algorithms	✓		✓				✓

Criteria for optimization													
References	Costing			Non-Costing			Risk assessment						
	Operating Cost	Non-Operating Cost	Room stability	Room capacity	Workload Capacity	Working days	Time Windows	Time	Idle Time	Consecutive Periods	AHP	BEN	SORA Standard
Bi et al. (2024)	✓			✓		✓		✓					
Mulumba and Diabat (2024)		✓	✓			✓		✓					
Eskandarpour and Boldsakhan (2023)	✓				✓					✓			
Kumbhar and Shin (2022)	✓			✓		✓		✓					
Arishi et al. (2022)	✓			✓		✓		✓					
Guo et al. (2023)		✓	✓			✓		✓					
Jiao et al. (2023)		✓				✓		✓					✓

Table 1 (continued)

References	Criteria for optimization											
	Costing			Non-Costing				Risk assessment				
	Operating Cost	Non-Operating Cost	Room stability	Room capacity	Workload Capacity	Working days	Time Windows	Idle Time	Consecutive Periods	AHP	BBN	SORA Standard
Kyriakakis et al. (2023)	✓				✓	✓			✓			
Sham et al. (2023)	✓		✓				✓					
Bhuiyan et al. (2022)	✓					✓	✓					
Hashemi et al (2022)	✓					✓	✓			✓		✓
Nguyen et al (2022)	✓			✓		✓	✓			✓		✓
Mahmoodi et al. (2022)		✓					✓					
Millar et al. (2023)	✓						✓				✓	✓
Dell'Amico et al. (2022)		✓	✓				✓	✓				
Vu et al. (2022)	✓					✓	✓		✓			
Liu et al. (2022)		✓	✓			✓	✓					
Gohari et al. (2022)	✓			✓		✓	✓			✓		✓
Chang and Laliberte (2023)		✓				✓	✓		✓			✓

Table 1 (continued)

References	Criteria for optimization												
	Costing				Non-Costing								
	Operating Cost	Non-Operating Cost	Room stability	Room capacity	Workload Capacity	Working days	Time Windows	Idle Time	Consecutive Periods	Risk assessment	AHP	BBN	SORA Standard
Wu et al. (2022)	✓				✓	✓		✓	✓				
Kong et al. (2023)	✓			✓		✓			✓		✓		✓
Nguyen et al (2022)		✓		✓					✓				
Sher and Sun (2023)	✓				✓	✓			✓				
Zhang et al. (2022)	✓				✓	✓		✓	✓				
Yu et al. (2022)	✓				✓	✓			✓				
Yang et al. (2023)	✓				✓	✓		✓	✓			✓	✓
Freitas et al. (2022)	✓				✓	✓			✓				
Sajid et al. (2022)	✓				✓	✓			✓				
Bi et al. (2023)	✓				✓	✓		✓	✓				
Our Article	✓		✓		✓	✓			✓			✓	✓
References	Criteria for optimization												
	Non-Costing												
	Battery Consumption			Perturbation		Travel distance		Room facilities		Robustness		Others	
Bi et al. (2024)	✓												
Mulumba and Diabat (2024)					✓								

Table 1 (continued)

References	Criteria for optimization									
	Non-Costing									
	Battery Consumption	Perturbation	Travel distance	Room facilities	Robustness	Others	Room facilities	Robustness	Others	
Eskandaripour and Boldsakhan (2023)			✓							✓
Kumbhar and Shin (2022)	✓									✓
Arishi et al. (2022)	✓	✓								✓
Guo et al. (2023)			✓							✓
Jiao et al. (2023)			✓							✓
Kyriakakis et al. (2023)			✓							✓
Sham et al. (2023)		✓								✓
Bhuiyan et al. (2022)	✓	✓		✓						✓
Hashemi et al (2022)			✓							✓
Nguyen et al (2022)	✓									✓
Mahmoodi et al. (2022)			✓							✓
Millar et al. (2023)										✓
Dell'Amico et al. (2022)		✓						✓		✓
Vu et al. (2022)			✓							✓
Liu et al. (2022)			✓							✓
Gohari et al. (2022)			✓							✓
Chang and Laliberte (2023)		✓								✓
Wu et al. (2022)			✓							✓
Kong et al. (2023)			✓							✓
Nguyen et al (2022)	✓	✓								✓
Shen and Sun (2023)		✓								✓
Zhang et al. (2022)			✓					✓		✓
Yu et al. (2022)		✓						✓		✓

Table 1 (continued)

References	Criteria for optimization							
	Non-Costing							
	Battery Consumption	Perturbation	Travel distance	Room facilities	Robustness	Others		
Yang et al. (2023)			✓		✓			
Fretas et al. (2022)		✓	✓	✓				
Sajid et al. (2022)	✓	✓			✓			
Bi et al. (2023)	✓		✓					✓
Our Article	✓		✓					✓

Distributor Locations (D): There are n potential locations where distributors can be stationed to facilitate UAV operations.

Facility Locations (F): There are m designated facilities that serve as operational hubs for managing and dispatching UAVs.

Demand Points or Customers (P): The system caters to the delivery demands of k distinct points, representing customers or delivery destinations.

UAVs (K): A fleet of L UAVs is available for conducting deliveries.

Recharging Points (D1): H demand points are identified as locations where UAVs can recharge during their operations.

Non-Recharging Points (D2): Q demand points are specified as locations where recharging is not possible, necessitating careful planning for energy conservation.

Scenarios (U): The system operates under three different scenarios, each representing a unique set of conditions or constraints that may influence the optimal configuration of routes and UAV assignments.

The optimization problem is multi-faceted, requiring a strategic approach to route planning, UAV allocation, and recharging station utilization. By strategically placing distributors and facilities, assigning UAVs judiciously, and navigating through the intricacies of recharging constraints at specific demand points, the aim is to minimize delivery times, reduce energy consumption, and enhance the overall sustainability of the UAV delivery system. This challenge is not only technologically demanding but also addresses practical considerations for real-world implementation. The outcome of this optimization endeavor has the potential not only to redefine last-mile logistics but also to contribute to a more sustainable and environmentally conscious approach to delivery services. As we delve into the complexities of optimizing a UAV delivery system within the outlined constraints, innovative solutions will pave the way for a future where unmanned aerial vehicles seamlessly navigate the skies, delivering goods efficiently and responsibly.

The primary challenge is to develop algorithms and strategies that optimize the delivery routes while considering the recharging constraints at specific demand points. This includes determining the most efficient distribution of UAVs among distributor and facility locations, minimizing delivery times, and ensuring that recharging points are strategically utilized to maximize the overall effectiveness of the UAV delivery system.

The optimization process must consider the diverse scenarios, accommodating variations in demand, operational conditions, and the recharging capabilities of the UAV fleet. The goal is to enhance the overall efficiency, reliability, and sustainability of the UAV delivery system within the specified framework.

3.2 Mathematical model

Based on the previous definitions, the model can be explained as Tables 2, 3 and 4. Also, in “Appendix A”, parameters initialization and values assignment details how parameters in a system or model are initialized and assigned values, including descriptions, initial settings.

Tables 2, 3 and 4 shows decision variables and parameters including point-specific values, service times, drone capacities, operational time windows, cost factors, battery-related parameters, and penalties associated with various operational conditions. Hence, the Python workflow for optimizing drone routing is presented, which encompasses phases such as importing libraries, setting up the environment, defining sets and scenarios, initializing parameters and decision variables, defining the objective function, setting constraints, assigning penalty values, and configuring a genetic algorithm for multi-objective optimization.

$$Z_1 = \min \sum_{k \in K} \sum_{d \in v_d} \sum_{j \in v} \sum_{i \in v} X_{ijkd} \cdot FC_k \cdot dx_{ij} \cdot C + W_2 \cdot \sum_{i \in P} E_i + W_3 \cdot \sum_{i \in P} L_i + \sum_{d \in D} \sum_{k \in K} Z_d \cdot fix_d + \sum_{d \in D} \sum_{k \in K} \sum_{i \in P} X_{dikd} \cdot fix'_k + \sum_{f \in F} Y_{df} \cdot de_d \cdot Cpf \quad (1)$$

The first objective function, denoted as Z_1 , aims to minimize the overall operational cost. This includes costs associated with drone transportation, battery usage along routes, fixed drone usage costs, cost for constructing distribution points at potential locations, penalties for not adhering to soft time windows, and preparatory expenses.

$$Z_2 = \min \sum_{u \in U} p_u \cdot \sum_{i \in P} s_{iu} + \lambda \sum_{u \in U} p_u \left(\sum_{i \in P} s_{iu} - \sum_{u \in U} p_u \sum_{i \in P} s_{iu} \right)^2 \quad (2)$$

The second objective function, denoted as Z_2 , seeks to minimize the service time. Since UAV velocity has different modes according to different routing scenarios while they are distinctive by the level of air traffic conditions. In a way, there is a set of U scenarios adjusted with possible routes which end in the set of j nodes. The number of scenarios is determined by experts who investigate the traffic conditions based on factors such as air parcels, severe climate, The National Aviation System (NAS) regulations, and so on, in the possible routes from nodes i to j .

Due to the uncertainty condition of scenarios, robust optimization is the appropriate method to estimate the solutions exactly. This optimization is done while unexpected conditions are considered and controlled. We used the Mulvey model (Mulvey et al., 1995) as the general form of robust optimization.

$$Z_3 = \min \sum_{i, j \in P \cup D} s_{ij}^k X_{ijkd} \quad (3)$$

The third objective function, labeled as Z_3 , is designed to reduce the risk index. This index is computed as the highest value among the sums of routing risks associated with each pair of nodes i and j , where i and j are part of the combined set $P \cup D$ (meaning, they belong to either P or D). The risk index is influenced by the aggregate of weighted components (factors) representing the routing risk for individual node pairs. The applied weighting method has been inspired from the (Mahmoodi et al., 2022) work. In their study, the SORA standard has been applied to estimate the imposed risk index, but, in this case, it has been tried to apply the BBN method to provide a risk index instead of the SORA approach. Concerning

Table 2 Defining sets: the foundation of optimization

Sets	Definitions
D	A set of distributor candidate locations
F	A set of facility locations
P	A set of demand points
K	A set of drones
D1	A set of demand points where recharging is possible
D2	A set of demand points where recharging is not possible
U	A set of different scenarios

Table 3 Defining parameters: the foundation of optimization

Parameters	Definitions
r_i	The amount of delivery demand of demand points i
P_i	The amount of pickup demand of demand points i
S_i	Time to provide service to demand points i
Q_k	Loading capacity of each RPA k
a_i	The earliest time allowed to provide service to distributor i in the hard time window
b_i	The latest time allowed to provide service to distributor i in the hard time window
M	Optional large number
ES_i	The earliest time allowed to provide service to distributor i in the soft time window
LS_i	The latest time allowed to provide service to distributor i in the soft time window
w_2	Cost per unit time deviation from the earliest time allowed in the soft time window
w_3	Cost per unit time deviation from the latest time allowed in the soft time window
fix_k^l	Fixed cost of using RPA k
C	Cost of one charging unit
AT	Minimum amount of charging allowed inside the RPA
Cf_f	Preparing cost of a unit in facility location f
fix_d	Cost of constructing distributor candidate location d
TS_i	Time to provide service to demand point i
DAY	The length of a working day
cp_{ji}	RPA battery consumption from node i to node j
dx_{ij}	The distance between node i and node j
$full$	Battery charging capacity
p_u	The probability of occurrence of scenarios u
V_{ku}	The velocity of RPA k in event u
cap_d	The capacity of candidate location of distributor d
\overline{cap}_f	The capacity of facility location f
LO_k	The load on RPA k when leaving the distributor
s_{ij}^k	The risk of route deriving from node i to node j with RPA k
x_{ijkd}	The variables zero and one. If RPA $k \in K$ belonging to candidate distributor locations d travels from node i to node j , it is equal to one and otherwise zero
s_{iu}	The time to start providing service to demand point i in scenario u
L_j	The weight of the load remaining on the RPA after service to demand point j
Z_d	The variables zero and one. If distributor d is constructed, it is equal to one and otherwise zero
E_{iu}	The time deviation from the earliest time allowed to provide service to demand point i in the soft time window in scenario u
L_{iu}	The time deviation from the latest time allowed to provide service to demand point i in the soft time window in scenario u

Table 3 (continued)

Parameters	Definitions
FC_k	The time to end the route of RPA k
de_d	The center demand of distributor d
Y_{df}	Variables zero and one. If distributor d is assigned to facility location f, it is equal to one and otherwise zero
A_i	The amount of battery available on the RPA
C_{ij}^k	ij Energy consumption by a drone of type k to fly from
C_k	C_k Amortized cost of the drone type k
C_{bat}^k	bat Amortized cost of the battery of drone type k
v	Drone speed
C_E	Cost of per unit of energy
C_L	Wage of a drone operators
n_k	Number of drones of type k a drone operator can operate
C_k^M	Maintenance cost of a drone of type k
t_k^{bat}	Time required to replace the battery of drone type k
l_i	Distance of delivery location i from depot
l_j	Distance of delivery location j from depot
t_{ij}	Time required for drone to arrive at delivery location from i to j
e_i	Earliest possible pickup time
ch_k^o	Initial energy in the battery of drone type k
ch_k^{min}	Minimum remaining energy required in the battery of drone type k
ch_k^{max}	Maximum remaining energy required in the battery of drone type k
Δch_j	Maximum permissible delay for point j
M_k^{max}	Maximum package weight carrying capacity of drone type k
M_i	Package weight for delivery location i

BBN methodology, it focuses on categorizing the risks associated with operating UAVs. The tool effectively integrates a wide variety of elements that may be responsible for the dangers and risks associated with UAV flight experiments. Through the BBN, one can visualize and numerically evaluate the causal relationships and influences affecting probabilistic outcomes by using Bayes' theorem to propagate causal probabilities across the whole system. We would like to investigate using this method for a full mission's safety assurance and assessment. Considering the important steps mentioned earlier, we apply the Analytic Hierarchy Process (AHP) ranking technique to assess the consequences of imposed risks by weighing them, in this way, the l_{ij}^k has been achieved according to the relation (3).

Table 4 Defining decision variables: the foundation of optimization

Decision variables	Description
x_{ijkd}	The variables zero and one. If RPA $k \in K$ belonging to candidate distributor locations d travels from node i to node j , it is equal to one and otherwise zero
Z_d	The variables zero and one. If distributor d is constructed, it is equal to one and otherwise zero
Y_{df}	Variables zero and one. If distributor d is assigned to facility location f , it is equal to one and otherwise zero
z_{ij}	1 if delivery location i is served immediately before j by a drone, 0 otherwise
y_i	1 if drone battery is replaced after returning from delivery location i , 0 otherwise
g_i	Remaining battery energy of a drone after returning from delivery location i
g_i^t	Auxiliary variable storing the remaining battery energy after returning from delivery location i
f_i	Timing of when a drone picks-up the package for delivery location i at depot
x_{ki}	1 if drone type k is assigned to deliver a package to location i , 0 otherwise
X_{Dji}	Binary variable indicating whether a route exists from the depot to i
X_{iDj}	Binary variable indicating whether a route exists from the j to depot
Y_{ij}	Binary variable indicating whether a drone travels from point i to a charging point j

3.2.1 BBN framework compatible with the established UAV network

BBN determine the significance of component s_{ij}^k depending on the perspective of the decision-makers. Nevertheless, it is important to remember that each risk factor stated is analyzed in the classification of SORA standard approach. Based on this methodology, risks categorized in two levels of aerial risk and ground risk. Based on this classification, all the incurred risks and their subcategories are categorized according to the origin of their occurrence. From this stage onwards, based on the BBN method, the parameter s_{ij}^k is obtained."

Which shows the level of significance of imposed risks For this purpose, Causing Risk Factor (CRF) identification starts after the BBN is formulated when qualitative indices are identified and classified according to AHP approach. At this point, based on the BBN model, a system is represented as a graphical representation of probabilities showing the level of dependence among the random variables in the system. This network has nodes that are variables, and arcs that connect them. Whenever there is an arc between two nodes, there is a causal relationship between them, while if there is none, there is no causal relationship between them. The parent nodes in this network are CRFs, and their subset of nodes is known as child nodes. It is possible for a node to be both a child and a parent node simultaneously. This study proposes a risk model according to BBN and the architectural elements of a network of semi-autonomous unmanned aerial vehicles that has three sub-layers. The mission of the UAV is managed automatically and manually in three sub-layers. These layers are the UAV, GBS, and Tender by humans to monitor and control UAVs' operation manually. Experts evaluate the potential risks in each of these levels (Han et al., 2022; Hashemi et al., 2021). The CRFs of the system are then identified and presented in a matrix format with the system dimensions as columns and risk levels as rows.

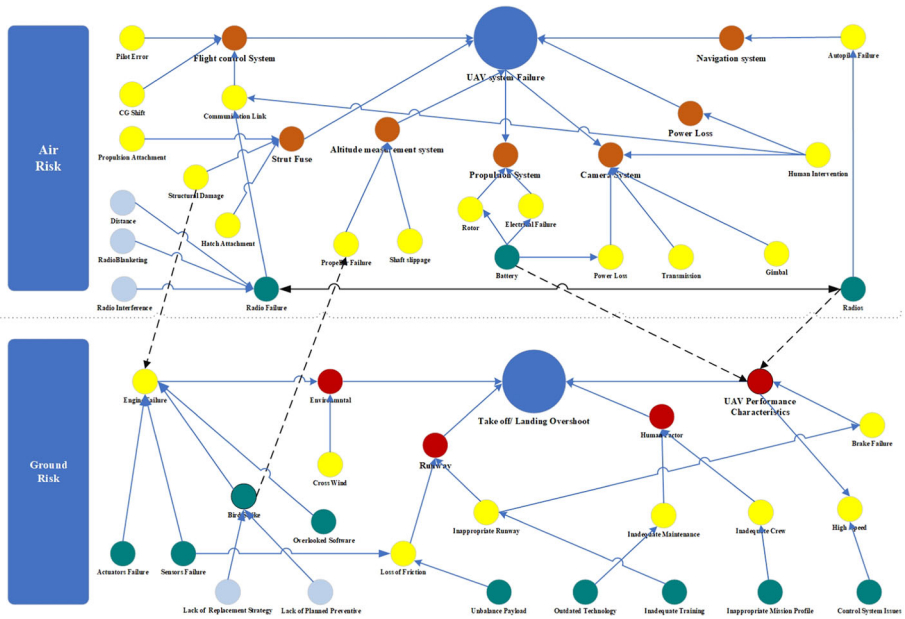


Fig. 1 Illustrative Bayesian network describing the inducements of UAV System in SORA standard classification

To create the BBN in this paper, a series of steps are taken:

1. The potential and essential occurrences and their effects on UAV missions are identified and chosen.
2. Detected events are assessed according to their primary CRFs and the degree to which those CRFs affect the event.
3. The CRFs are ranked according to their significance, which reflects their level of reliance. A dependence graph is created with no return paths between the nodes of the graph and with direct causal connections between them.
4. At this point, the BNN is represented by a conditional probability table (CPT). This table is generated considering the outcome anticipated from the presence of the CRFs and aggregation of experts' opinions.
5. The proportionality of the evaluation of the solution for modifying and eliminating each potential risk and its potential impact on enhancing the system's safety is considered.
6. Subsequently, at each risk level in the BNN graph, the overall risk level is determined based on the computed likelihood of a mishap for each CRF.

An illustration of this sensitivity evaluation can be seen in Fig. 1 (Bareither & Luxhøj, 2007; Millar, 2015).

Figure 2 illustrates the CRFs for the risk level of a UAV system and its connections. The same process depicted in Fig. 2 is applied to calculate all the CRFs for the remaining detected events.

According to the recorded statistical results from the data analysis and the literature (Washingtona et al., 2017; Kevorkian et al., 2016; Millar, 2015; Allouch et al., 2019; Han et al., 2020), the BNN graph showing the failure of a UAV system can be seen in Fig. 2.

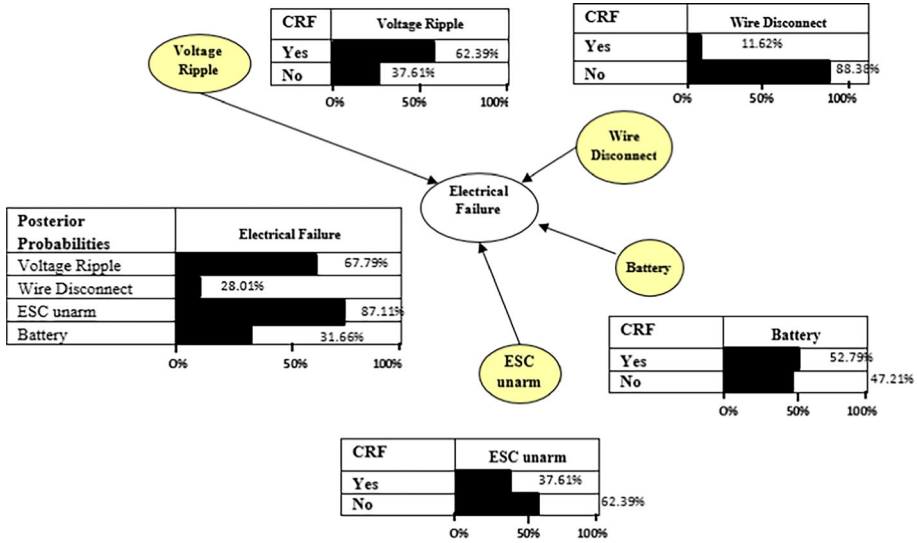


Fig. 2 Illustrative Bayesian network describing the inducements of UAV System Failure

The CPT can then be calculated by measuring the strength of connections between the nodes. The output of the CPT in this state is as follows if the variables, or system elements, are in the form of the set $N = \{n_1, \dots, n_r\}$:

$P(n_q|\pi_q)$ denotes the likelihood that each node n_q will exist if a set of π_q parents are available for it. Based on their relationship with their parents, this conditional probability is determined (Noriega et al., 2019). Figure 1 shows a computed example based on a BBN graph of Fig. 2 and an electrical failure intermediate event from CPT. In this table, conditional probabilities are calculated using Eqs. (4) and (5):

$$P(n_1, \dots, n_r) = \prod_{q=1}^r P(n_q|\pi_q) \tag{4}$$

$$p(n_q|\pi_q) = \frac{p(\pi_q|n_q) \cdot p(n_q)}{p(\pi_q)} \tag{5}$$

Many parents result in a tremendous amount of cognitive load for experts in this domain, as they must calculate the conditional probability of all parent variables by comparing their probability distribution with that of the number of child nodes. Additionally, every conditional probability is determined by the domain expert’s personal experience and reflects their subjective probability. This Knowledge is influenced by experience and biases based on individuals’ experiences (Das et al., 2004).

In every episode of UAV action in the predefined plane ψ , the risk index s_{ij}^k relies on the average of the CRFs that experts determine for the candidate range of the next actions from the origin point (UAV) n to the destination point (Tender) m in the episode.

ace, experts evaluated each CRF. In fact, $N_1 \times N_2$ squares, which correspond to the size of a time slot, divide the possible zone, thus at this stage, the experts select a set of these squares as a specific area and provide their assessment of the probable risk index for these predefined areas. The weights of each identified risk indicator are assessed using AHP to ensure that

the opinions of the experts are not inconsistent. In accordance with the recorded data, events occurred in different risk categories and had various probabilities, so expert opinions can change from one period to the next.

$$Z_4 = \min C_E \left(\sum_{i \in P} \sum_{j \in P} C_{ij}^k z_{ij} \right) + \left(C_k + \frac{C_L}{n_k} + C_k^M \right) \sum_{j \in P} z_{0j} + C_{bat}^k \left(\sum_{i \in P} y_i \right) \quad (6)$$

The fourth objective function, denoted as Z_4 , aims to minimize the overall expenditure associated with the following components: total energy consumption cost (component 1), total investment and operational expenses for the drones (component 2), and investment costs related to the batteries (component 3). This optimization is conducted to efficiently deliver all customer orders while adhering to specified pickup time windows within the planning horizon.

Subject to:

$$\sum_{d \in D} \sum_{k \in K} \sum_{i \in P \cup D} X_{ijkd} \geq 1, \forall j \in P \quad (7)$$

$$\sum_{i \in D \cup P} X_{ijkd} = \sum_{i \in D \cup P} X_{jikd}, \forall d \in D, k \in K, j \in P \quad (8)$$

$$\sum_{d \in D} \sum_{i \in v} X_{dikd} \geq 1, \forall k \in K \quad (9)$$

$$X_{iikd} = 0, \quad \forall d \in D, k \in K, i \in D \cup P \quad (10)$$

$$S_{iu} + \frac{dx_{ij}}{V_{ku}} - M \cdot (1 - X_{ijkd}) \leq S_{ju}, \forall d \in D, k \in K, i \in D \cup P, j \in P, u \in U \quad (11)$$

$$S_{iu} + \frac{dx_{ij}}{V_{ku}} + M \cdot (1 - X_{ijkd}) \geq S_{ju}, \forall d \in D, k \in K, i \in D \cup P, j \in P, u \in U \quad (12)$$

$$S_{du} = 0, \forall d \in D, u \in U \quad (13)$$

$$a_i \leq S_{iu} \leq b_i, \forall i \in P, u \in U \quad (14)$$

$$LO_k = \sum_{d \in D} \sum_{i \in v} \sum_{j \in P} r_j \times X_{ijkd}, \forall k \in K \quad (15)$$

$$LO_k \leq Q_k, \forall k \in K \quad (16)$$

$$L_j \geq LO_k - r_j + p_j - M \cdot (1 - X_{djkd}), \forall d \in D, k \in K, j \in P \quad (17)$$

$$L_j \leq LO_k - r_j + p_j + M \cdot (1 - X_{djkd}), \forall d \in D, k \in K, j \in P \quad (18)$$

$$L_j \geq L_i - r_j + p_j - M \cdot \left(1 - \sum_{d \in P} \sum_{k \in K} X_{ijkd} \right), \forall j \in P, \forall i \in D \quad (19)$$

$$L_j \leq L_i - r_j + p_j + M \cdot \left(1 - \sum_{d \in P} \sum_{k \in K} X_{ijkd} \right), \forall j \in P, \forall i \in D \quad (20)$$

$$L_j \cdot \left(\sum_{d \in D} \sum_{i \in P \cup D} X_{ijkd} \right) \leq Q_k, \forall j \in P \quad (21)$$

$$E_{iu} \geq \alpha (ES_i - S_{iu}), \forall i \in P, u \in U \quad (22)$$

$$L_{iu} \geq \beta(S_{iu} - LS_i), \forall i \in P, u \in U \tag{23}$$

$$A_i = \text{full}, \forall i \in D_1 \tag{24}$$

$$A_i \leq A_j - DX_{ji} \cdot FC_k + M \cdot (1 - X_{jkd}), \forall i \in D_2, j \in P \cup D, k \in K, d \in D \tag{25}$$

$$A_i \geq AT, \forall i \in P \tag{26}$$

$$Z_d \cdot M \geq \sum_{k \in K} \sum_{i \in P} X_{dikd}, \forall d \in D \tag{27}$$

$$\sum_{f \in F} Y_{df} \geq 1, \forall d \in D \tag{28}$$

$$de_d = \sum_{k \in K} \sum_{i \in P \cup D} \sum_{j \in P} de_d \times X_{ijkd}, \forall d \in D \tag{29}$$

$$de_d = cap_d, \forall d \in D \tag{30}$$

$$\sum_{f \in F} \sum_{d \in D} Y_{df} \cdot de_d \leq \overline{cap}_f, \forall f \in F \tag{31}$$

$$FC_k \geq S_{iu} + \frac{dx_{id}}{V_{ku}} - M \cdot (1 - X_{idkd}), \forall k \in K, i \in P, d \in D, u \in U \tag{32}$$

$$\sum_{k \in K} \sum_{i \in P \cup D} \sum_{j \in P} S_i \times X_{ijkd} \leq DAY, \forall k \in K \tag{33}$$

$$X_{ijkd}, Z_d, Y_{df} = 0 \text{ or } 1 \tag{34}$$

$$L_j, S_{iu}, LO_{dk} \geq 0 \tag{35}$$

$$s_{ij}^k \leq M \sum_{i \in P \cup D} X_{jikd}, \forall j \in P, k \in K \tag{36}$$

$$s_{ij}^k \leq M \sum_{i \in P \cup D} X_{ijkd}, \forall j \in P, k \in K \tag{37}$$

$$s_{ij}^k = 0, \forall j \in D, k \in K \tag{38}$$

$$\sum_{i \in P} z_{ij} \geq 1, \forall j \in P \tag{39}$$

$$\sum_{j \in P} z_{ij} \geq 1, \forall i \in P \tag{40}$$

$$\sum_{i \in P} z_{ij} = \sum_{i \in P} z_{ji}, \forall j \in P \tag{41}$$

$$\sum_{i \in P} c_{ij}^k z_{ij} \leq (ch_k^0 - ch_k^{\min}), \forall j \in P \tag{42}$$

$$M_j \sum_{i \in P} z_{ij} \leq M_k^{\max}, \forall j \in P \tag{43}$$

$$f_j \geq f_i + (t_l + t_{ij} + t_u) + t_k^{bat} y_i - M(1 - z_{ij}), \forall i, j \in P, i \neq j \tag{44}$$

$$e_i \leq f_i \leq l_i, \forall i \in P \tag{45}$$

$$\sum_{j \in P} g_j^t + \sum_{j \in D_1} \Delta ch_j \leq ch_k^0 - \sum_{i, j \in P} c_{ij}^k \cdot X_{ijkd} \quad (46)$$

$$ch_k^0 - \sum_{i, j \in P} c_{ij}^k \cdot X_{ijkd} \geq ch_k^{min} \quad (47)$$

$$ch_k^0 - \sum_{i, j \in P} c_{ij}^k \cdot X_{ijkd} + \sum_{j \in D_2} \Delta ch_j \leq ch_k^{max} \quad (48)$$

$$g_j \leq ch_k^0 - \sum_{i, j \in P} c_{ij}^k \cdot X_{ijkd} \quad (49)$$

$$z_{ij} \in \{0, 1\}, \forall i, j \in P, i \neq j \quad (50)$$

$$g_i \geq 0, \forall i \in P \quad (51)$$

$$g_i^t \geq -ch_k^{min}, \forall i \in P \quad (52)$$

$$f_i \geq 0, \forall i \in P \quad (53)$$

$$\min \sum_{i \in P} \sum_{k \in K} c_{ij}^k \cdot x_{ki} \quad (54a)$$

$$s.t., \sum_{k \in K} x_{ki} = 1, i \in P \quad (54b)$$

$$c_{ij}^k \cdot x_{ki} \leq (ch_k^0 - ch_k^{min}), \forall k \in K, \forall i \in P \quad (54c)$$

$$M_i \cdot x_{ki} \leq M_k^{max}, \forall i \in P, k \in K \quad (54d)$$

$$x_{ki} \in \{0, 1\}, \forall i \in P, k \in K \quad (54e)$$

$$\begin{aligned} &\text{if } e_i + t_l + t_{ij} + t_u > l_i \\ &\text{then } z_{ij} = 0, \forall i, j \in P \end{aligned} \quad (55)$$

$$\begin{aligned} &\text{if } l_j > l_i + t_{ij} + 2(t_l + t_u + 2t_{Range}) \\ &\text{then } z_{ij} = 0, \forall i, j \in P \end{aligned} \quad (56)$$

$$\sum_{j \in P} X_{Dji} = 1, \forall i \in P \quad (57)$$

$$\sum_{j \in P} X_{iDj} = 1, \forall j \in P \quad (58)$$

$$\sum_{j \in D_1} Y_{ij} \geq 1, \forall i \in P \setminus D_1 \quad (59)$$

$$g_i + \Delta ch_j \leq ch_k^{max}, \forall j \in D_1 \quad (60)$$

The sophisticated framework of constraints within the UAV logistics system underscores its multifaceted approach to enhancing operational efficiency and flexibility. Constraints (7) through (10) are pivotal in allocating UAVs to demand points with enhanced flexibility, ensuring efficient service even when the demand requires multiple drones at a single point. This set includes mandates for UAV allocation to specific demand points, the use of UAVs by multiple distributors, and the prevention of redundant routing paths. Following closely, constraints (11) through (16) focus on the initiation phase of UAV operations, including service

start times and initial load capacities. These constraints are designed to set the operational groundwork, ensuring UAVs begin their routes efficiently and are prepared for their delivery tasks.

The subsequent section delves into the UAVs' operational constraints during their delivery routes, with constraints (17) through (26) meticulously calculating load weights and ensuring adherence to the UAV's battery and capacity limitations. This segment emphasizes the importance of maintaining operational integrity throughout the UAV's journey, from departure to service completion at demand points. Particularly, constraints (24) through (26) highlight the critical aspect of battery management, ensuring UAVs operate within their energy capacities, which is vital for sustaining longer operational periods and enhancing reliability.

To optimize the distribution network and resource allocation, constraints (27) through (33) introduce the construction and association of distribution centers (DCs) with facility locations, alongside evaluating demand restrictions and travel times. This part of the model enhances the flexibility and effectiveness of facility allocation within the network, ensuring that demand is aligned with available resources and that UAV travel times are optimized for efficiency. These constraints collectively aim to bolster the logistical backbone of the UAV delivery system, ensuring that distribution centers and UAVs are strategically aligned with the overarching goals of operational efficiency and resource optimization.

Finally, the model extends its meticulous planning to route safety, delivery efficiency, and energy management with constraints (34) through (60). This includes binary decision-making for travel routes, ensuring energy consumption remains within operational limits, and mandating that every delivery route originates and concludes at the depot to maintain a centralized routing strategy. Particularly noteworthy are constraints (46) through (60), which focus on energy management and the strategic scheduling of pickups and deliveries to ensure timely and efficient operations. The overarching aim, encapsulated in constraints (54a) to (54e), is to minimize total energy consumption while aligning operational efficiency with the practical capabilities of the drones. This comprehensive set of constraints ensures that the UAV logistics system operates within a framework designed to maximize efficiency, safety, and reliability, thereby optimizing the delivery process in an innovative and forward-thinking manner.

4 Solution approach

To have a comprehensive analysis of NSGAI algorithm performance, the optimal flight path has been obtained through the developed Genetic algorithm. In this case, since the whole flight space is considered a grid network, UAVs start their mission in a set of $N_e \times N_f$ small squares in this network. In the GA, each chromosome represents the sequence of paths between the hypothetical start point to the endpoint. Selection of the best path is applied for the whole chromosome with respect to the value of the proposed four objective functions. Hence, the next generation of chromosomes will be the all-possible routes between the N_{ef} to its neighboring sequence, the N_{e+1f+1} , which are identified as R_{ef} . Crossover and mutation operators have been applied to produce next generation from parent squares because their visiting order is completely relied on the degree of optimality of objectives in the selected square. Their concerned values are depicted in table A2. Figure 3 show m strings of chromosome and crossover strategy of the proposed GA algorithm. In the sequence of chromosome some squares highlighted as potential nodes in the UAV networks, between the adjacent nodes, random sequence of possible path cells exists. GA begins with initial

population of chromosome in this shape of structure, they follow the steps of objectives evaluation, applying genetic operators and regeneration at the end.

Every chromosome which is made in child generation is evaluated by the proposed objectives of the model. Then the chromosome with the optimal values is targeted as the best flight path for UAVs. According to the multi-objective model in metaheuristic algorithm, best solutions are the category of points in the Pareto front in which none of them will triumph over the other for any of the objective functions and a solution is superior when at least one of the objectives has an optimal value.

To address the multi-objective optimal allocation problem, formulated as a mixed-integer non-linear program (MINLP), we propose employing the non-sorting genetic algorithm (NSGA-II) as outlined in the flowchart in Fig. 4. The primary advantage of this method is that NSGA-II concurrently optimizes each objective. NSGA-II is a widely used and efficient sorting multi-objective genetic algorithm capable of handling non-penalty constraints. It exhibits fast and effective convergence, making it well-suited for large-scale searches and proficient at addressing problems that initiate with a non-feasible solution. The proposed algorithm involves multiple layers of individual classifications, where non-dominated individuals receive a specific dummy fitness value before being removed from the population. This process iterates until the entire population is classified. NSGA-II offers advantages such as introducing elitism to NSGA and preserving diversity within a fast and less complex algorithm.

In a more detailed breakdown, NSGA-II undertakes the selection of the optimal number of UAVs, their appropriate battery sizes, the designated charging point (starting point), and the assignment of buses to each UAV. Additionally, the algorithm allocates these buses to specific trips, determining the optimal number of buses to be monitored and their respective locations. Subsequently, all these selections are fed into the fitness calculation of NSGA, which comprises two distinct parts.

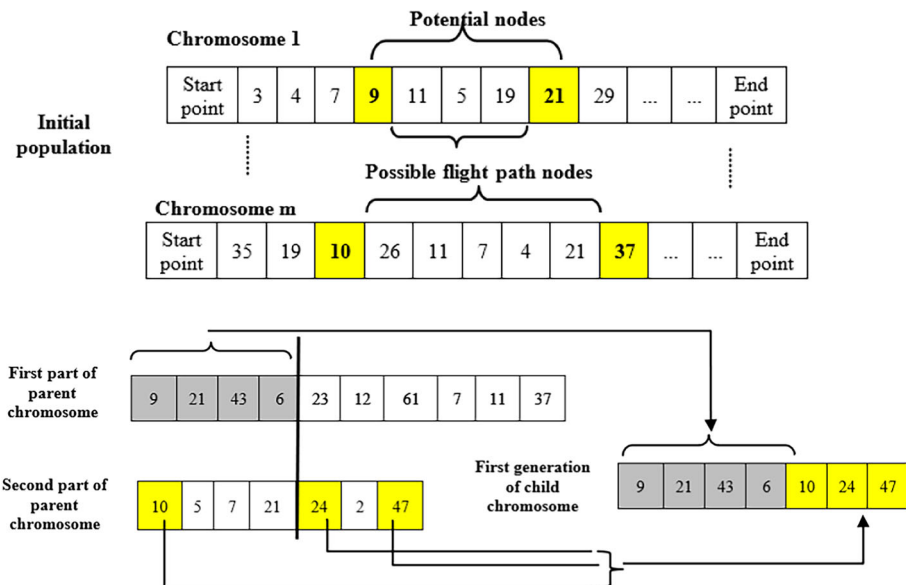


Fig. 3 The proposed crossover strategy

The first part is responsible for calculating the loss of observability (objective one) and takes the number of buses to be monitored and their locations as inputs. The second part is tasked with computing the total annual cost (objective two), with inputs including the selection of the number of UAVs, their appropriate battery sizes, their designated charging point (starting point), and the assigned buses to each UAV. Within the second part, an internal subproblem arises to derive the optimum route for each trip.

Following the calculation of the optimal route for each trip, NSGA utilizes the selected route and battery specifications to check the constraints for each trip. Specifically, it verifies that the maximum hovering and flying power are less than or equal to the selected battery’s power consumption (as in Eq. (6)). Furthermore, the consumed energy must be less than or equal to the actual useful energy of the battery, as stipulated in Eq. (6).

NSGA-II employs a robust elitism approach, combining parent and offspring populations to create tiers based on non-dominance, organizing solutions into several fronts. Each front categorizes solutions based on their level of dominance, starting with non-dominated solutions and proceeding to those dominated by progressively more solutions. Within each front, solutions are further sorted by crowding distance, a measure of the spacing between solutions, to ensure diversity. This dual sorting method—by dominance level and crowding distance—facilitates the selection process, prioritizing non-dominated solutions and, among those of equal dominance, the ones with greater spacing. The algorithm continually evolves through

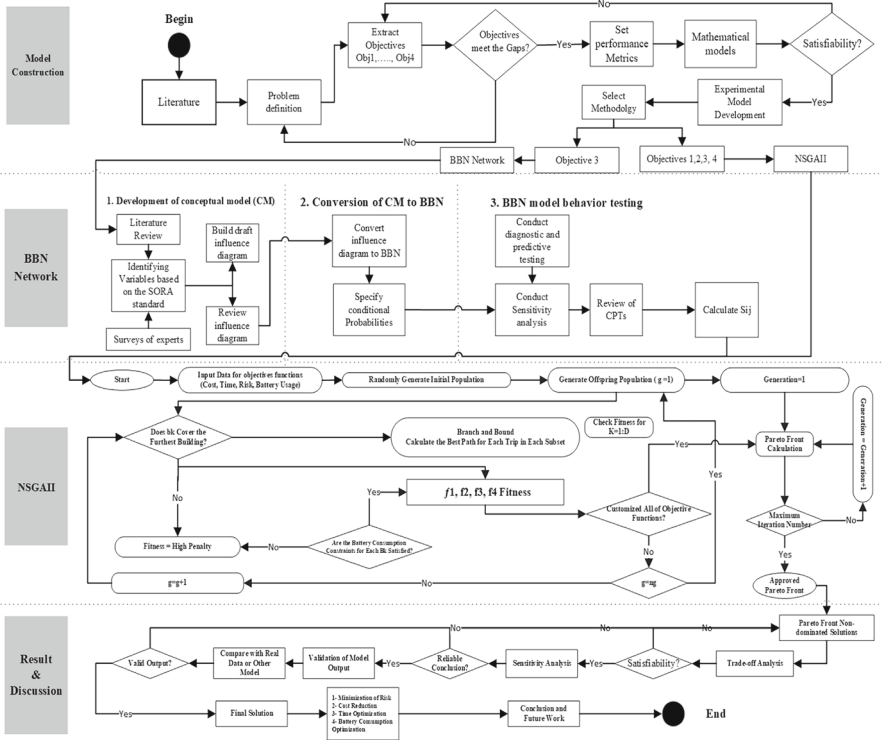


Fig. 4 Displays the flowchart for the suggested NSGA-II algorithm

Procedure NSGA-II with BBN Integration for Parameter s_{ij}^k	
Inputs:	
N:	Population size
g:	Number of generations
f:	List of objective functions
Output:	
The final population after g generations	
Begin	
1:	Initialize Population P with size N
2:	Infer s_{ij}^k for the third objective function using Bayesian Belief Network (BBN)
3:	Evaluate objectives for P using inferred s_{ij}^k
4:	Sort P based on non-dominance into fronts, assign ranks
5:	for i = 1 to g do
6:	Generate Child Population Q from P
7:	Apply genetic operators - Recombination and Mutation
8:	Combine Parent and Child populations to form R
9:	Infer s_{ij}^k for R using BBN
10:	Evaluate objectives for R including the third objective using s_{ij}^k
11:	Sort R based on non-dominance into fronts, assign ranks
12:	Calculate crowding distance for individuals in each front
13:	Select the next generation population P from R based on rank and crowding distance until size N is filled
14:	End For
End	

Fig. 5 Pseudocode of NSGA-II

selecting the fittest solutions, followed by their recombination and mutation, to generate new populations. The pseudocode NSGA-II can be seen in Fig. 5.

5 Results and discussions

This section outlines the experimental studies conducted. All algorithms are coded in Python and implemented on a 64-bit Windows OS with Intel Core (TM) i7-10700, 2.9 GHz, and 32 GB RAM. These following results are obtained using NSGAI (Non-dominated Sorting Genetic Algorithm II) with the following parameters:

Population: 120 individuals

Number of Generations (Iterations): 100 generations

Crossover Probability (CXPB): 0.7

Mutation Probability (MUTPB): 0.1

Independent Probability (indpb): 0.1

Table 5 Comprehensive analysis of optimal parameters for drone routing

Index	Cost	Time	Risk	Battery Usage	Penalties
Count	28	28	28	28	28
Mean	116,393	19	345	312	2748
Std	15,358	2	123	479	119
Min	87,480	19	204	100	2555
25%	105,666	19	276	181	2675
50%	116,074	19	295	220	2730
75%	129,754	19	450	268	2835
Max	139,887	28	605	2734	2900

5.1 Summary and descriptive analysis

5.1.1 Table of statistics

The Table 5 provides a succinct summary of the dataset across five different variables: Cost, Time, Risk, Battery Usage, and Penalties. With a count of 28 for each variable, there is a sufficient sample size to understand the trends and distributions within the data. The mean cost is relatively high at 116,393, but it is important to consider the standard deviation, which at 15,358, suggests a moderate spread around the mean. This spread indicates variability in costs, which could be due to a range of factors that would require further investigation. The 'Time' variable exhibits a narrow standard deviation, indicating that this measurement is uniform throughout the dataset, which denotes a consistent performance on this metric. The parameters governing the time objective function, namely 'pu' and 'siu', were assigned values that are nearly identical across various points and scenarios. As a result, this uniformity in parameter settings has led to the reduced variability in 'Time'. 'Battery Usage' presents with the largest standard deviation relative to its mean, indicating very high variability. This is further highlighted by the maximum value, which is significantly higher than the 75th percentile, suggesting the presence of outliers that dramatically affect the average. For 'Penalties', the lower standard deviation indicates that penalties do not vary as much as some of the other variables, such as 'Battery Usage', but there is still a noticeable range between the minimum and maximum values.

5.1.2 Table of non-dominated individuals

The Table 6 illustrates the best-performing individuals based on the criteria that no other individual is better in all the objectives. These are essentially the solutions that offer the best trade-offs among the objectives considered. For instance, Index 0 has a high cost but compensates with lower risk and penalties, while Index 4 has the highest risk but does not have the highest cost or penalties, which may suggest it is a viable option under certain circumstances where risk is less of a concern. It is important to note the presence of significant variation in 'Battery Usage' and 'Risk' among the non-dominated individuals, which indicates that the trade-offs between these two variables are quite substantial and likely to be a focal point in decision-making processes. The consistency of the 'Time' across most non-dominated individuals suggests that it is not a differentiating factor in the optimization process. Moreover,

some individuals like Index 14 show an extremely high 'Battery Usage', which is an outlier that could be a result of specific operational requirements or an error in data recording. This kind of outlier needs special attention as it can skew the overall analysis and may represent a special case that is not generalizable. From the summary statistics, it becomes evident that 'Cost' and 'Risk' are variables with high variability, suggesting a varied dataset where each observation might represent different operational scenarios or decision contexts. The 'Battery Usage' variable, particularly, with its high variability and extreme maximum value, requires closer scrutiny to understand the underlying factors causing such discrepancies. The analysis of non-dominated individuals provides insights into the complex trade-offs between different objectives. It highlights the potential for multiple optimal solutions depending on the weightings of various objectives, such as cost, risk, and battery usage. In interpreting

Table 6 Non-dominated individuals—identifying optimal solutions with superior trade-offs across multiple objectives

Index	Cost	Time	Risk	Battery Usage	Penalties
0	129447	28	400	183	2555
1	130676	19	315	175	2710
2	103888	19	450	263	2835
3	125911	19	204	281	2675
4	103782	19	605	281	2835
5	139887	21	450	100	2780
6	138876	19	204	234	2555
7	108258	19	491	234	2745
8	136199	19	276	175	2900
9	114315	19	605	124	2900
10	127436	19	205	183	2835
11	107547	19	205	307	2675
12	117832	19	276	183	2715
13	139160	19	205	183	2715
14	126518	19	450	2734	2590
15	87480	19	495	183	2715
16	107329	19	276	229	2900
17	132499	19	276	234	2555
18	105449	19	315	175	2900
19	108782	19	276	211	2675
20	118152	19	315	151	2790
21	107496	19	276	253	2835
22	89029	21	400	406	2675
23	93556	19	276	307	2675
24	119603	27	276	341	2555
25	105738	19	491	151	2900
26	131441	19	204	199	2835
27	102721	19	450	250	2900

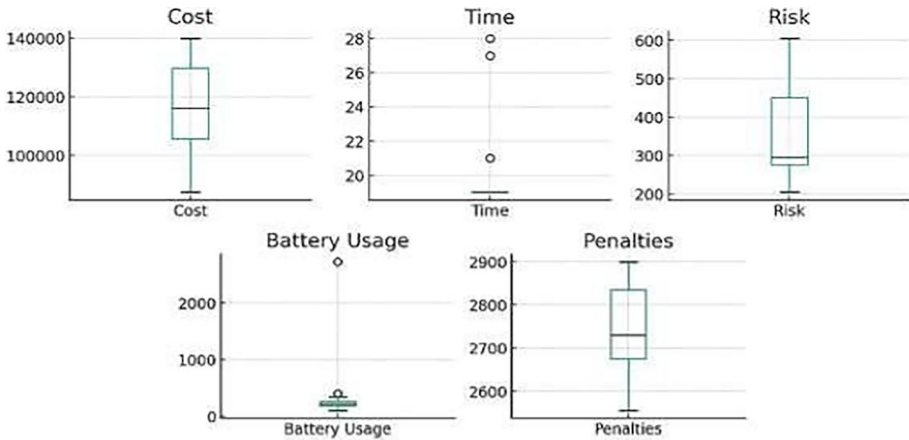


Fig. 6 Objective functions penalties distribution

these results, it is crucial to consider the context in which the data was collected, as the importance and impact of each variable may vary significantly across different operational environments. Additionally, the presence of outliers suggests that there may be extreme cases that are significantly different from the norm, and these warrant separate analysis to ensure they do not distort the overall understanding of the data. Ultimately, this analysis lays the groundwork for a deeper exploration into the factors that drive these variables and how they can be managed or optimized in the specific context from which the data is drawn.

5.2 Data distribution

5.2.1 Box plots for objectives and penalties

The Fig. 6 for box plots for 'Cost', 'Time', 'Risk', 'Battery Usage', and 'Penalties' provide a visual summary of the distribution and variability of these variables within the dataset.

- **Cost:** The box plot for 'Cost' shows a median around 116,000, with the interquartile range (IQR) indicating that the middle 50% of costs are tightly packed. This suggests a moderate consistency in cost across the dataset, with a few outliers indicating instances of significantly higher costs.
- **Time:** 'Time' presents with a very narrow IQR, and all but three data points are identical. The outliers suggest only occasional variation from a standard time value, which implies that the duration of the observed activities or processes is generally consistent.
- **Risk:** The 'Risk' variable has a wider IQR, demonstrating more variability in the dataset's risk levels. The presence of upper outliers indicates that there are scenarios with substantially higher risk, although the bulk of the data is less variable.
- **Battery Usage:** This box plot is particularly notable for the extreme outlier, which is significantly higher than all other observations. This suggests a special case within the dataset where battery usage is exceptionally high compared to the norm.
- **Penalties:** The 'Penalties' distribution is relatively symmetrical with a slight skew towards the upper end, indicated by a median that is closer to the lower quartile. This suggests that while there is some variation in penalties, it does not vary as extremely as battery usage.

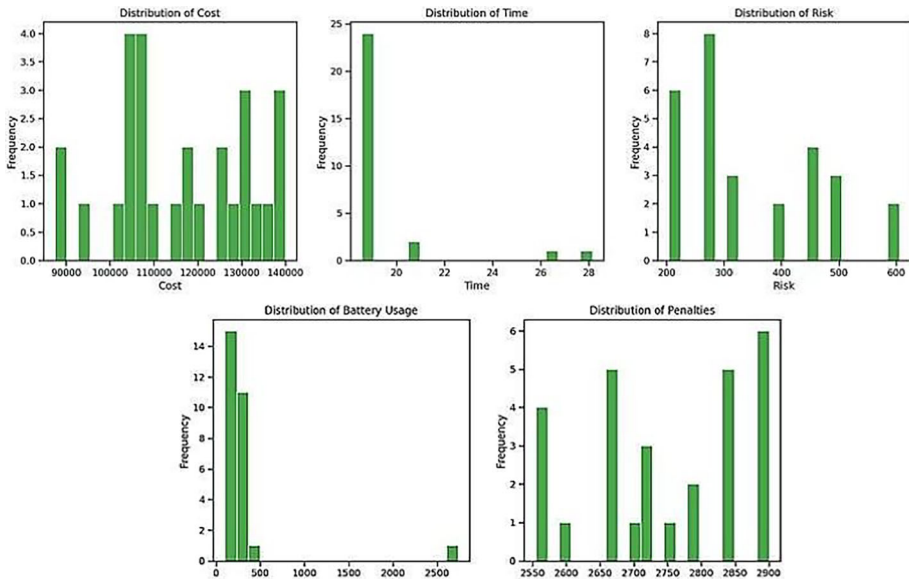


Fig. 7 The frequency distribution of the dataset's variables. The provided histograms offer a visual representation of the frequency distribution of the dataset's variables: Cost, Time, Risk, Battery Usage, and Penalties

These box plots are critical for understanding the underlying distributions of each variable, identifying outliers, and assessing the spread and symmetry of the data. Outliers warrant further investigation to determine whether they represent data recording errors, special cases, or if they are a part of the natural variability in the dataset. The relatively stable 'Time' variable contrasts with the high variability seen in 'Risk' and 'Battery Usage', which could imply that different factors or levels of control affect these areas. This kind of analysis is instrumental for developing strategies to manage or optimize each objective and penalty within the given operational context.

5.2.2 Distribution of objectives and penalties

The Fig. 7 presented show how often each value or range of values occurs within the dataset for five variables: Cost, Time, Risk, Battery Usage, and Penalties. Each histogram's horizontal axis represents the possible values or ranges for a variable, while the vertical axis indicates how frequently these values occur. This visual analysis helps to understand the distribution and central tendencies like the mean or median, and the variability or spread of the data for each variable, aiding in further statistical analysis or modeling. The detailed explanation of each section is provided below:

- **Cost:** The histogram for Cost shows a relatively even distribution across several bins, with frequencies tapering off as the cost increases. This indicates a range of cost values within the dataset, with fewer instances of very high costs.
- **Time:** The Time distribution is highly skewed, with most observations clustered around a single value, which indicates very little variation in the time metric across different observations. The few occurrences of higher time values are outliers.

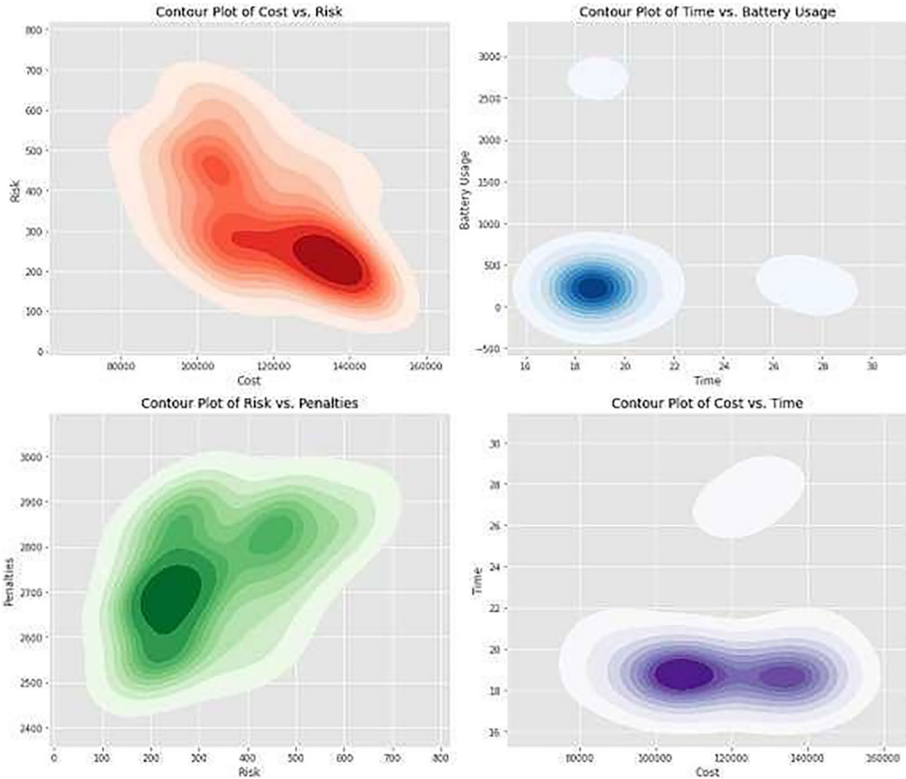


Fig. 8 Comparative contour plots of objectives

- **Risk:** The Risk histogram displays a multi-modal distribution with several peaks, suggesting that certain risk levels occur more frequently than others. This could point to common risk profiles within the operational context from which the data was collected.
- **Battery Usage:** The Battery Usage distribution is highly skewed with one significant outlier, which suggests that one observation or set of conditions led to an unusually high battery usage. This outlier could potentially be an area of concern or interest for further investigation.
- **Penalties:** The Penalties distribution appears to be bi-modal, with two peaks suggesting that there are two common penalty values within the dataset. This could indicate the presence of two distinct groups or conditions under which penalties are typically incurred.

5.3 Density analysis

5.3.1 Contour plots

The figure 8 indicated a visual narrative for the interplay between paired variables, revealing the density and distribution that might not be as apparent through numerical analysis alone. In the interrelation of cost and risk, the data congregates within a middle ground, suggesting a balanced operational approach where neither extreme cost nor high risks are prevalent. This

pattern is a testament to an underlying strategy that might be prioritizing cost-efficiency up to a certain threshold of acceptable risk. This strategic balance is disrupted when considering the battery usage outliers, which stand apart in the contour plot of time versus battery usage. The stark isolation of these outliers indicates exceptional cases, perhaps indicative of atypical scenarios or data anomalies, which starkly contrast with the otherwise homogenous spread signifying operational standardization. Furthermore, the risk versus penalties contour plot intimates a correlation where moderate risks are commonly paired with proportionate penalties. The plot unveils a central tendency in the data, suggesting a predictive nature of penalties based on risk levels, which could be a valuable insight for risk mitigation strategies. Similarly, cost and time exhibit a relationship that is clustered around specific values, reinforcing the notion of standard. Operating times across varied costs. The existence of these clusters points to established procedures and a potential efficiency ceiling that might be explored for further optimization. The collective insights from these contour plots are instrumental for strategic planning. They highlight the prevailing operational regimes, while also flagging outliers and anomalies for further inquiry. Such visual tools allow for an aggregated comprehension of complex data interactions, laying the groundwork for refined resource management and more targeted risk control measures. In addition to the detailed explanation provided in the article, the contour plots in Fig. 8 offer further insights:

1. **Cost versus Risk:** The plot reveals a concentration of data in a specific range, indicating an operational preference for balancing moderate costs and risks. This suggests a tactical approach where cost and risk are managed to avoid extremes, enhancing operational stability.
2. **Time versus Battery Usage:** Notable outliers in this plot signify unusual cases that deviate significantly from the norm, pointing to potential anomalies or special operational scenarios that require further investigation.
3. **Risk versus Penalties:** The data suggests a direct relationship between risk and penalties, where moderate risks correspond to proportionate penalties, providing a basis for predictive risk management and mitigation strategies.
4. **Cost versus Time:** The clustering around particular values suggests a standardized operating time for various costs, indicating potential efficiency limits that could be optimized further.

These visual insights are crucial for strategic planning, highlighting standard operational regimes and identifying outliers for focused analysis, thus aiding in refined resource management and targeted risk control measures.

5.4 Relationship and correlation analysis

5.4.1 Heatmap of data correlation

The Fig. 9 presented the heatmap of objective correlations offers a compelling visual guide to the relationships between various operational metrics. Each square on the heatmap represents the correlation coefficient between two variables, ranging from -1 to 1 . A value of 1 indicates perfect positive correlation, -1 indicates perfect negative correlation, and 0 denotes no correlation. In this heatmap, the correlation between cost and risk stands out with a coefficient of -0.40 , suggesting a moderate negative relationship. This could imply that as cost decreases, risk might increase, or vice versa, pointing towards a trade-off between these two objectives where a balance might be sought. The relationship between time and penalties is also notable, marked by a correlation coefficient of -0.45 . This suggests that longer times

might be associated with fewer penalties, or shorter times could correlate with increased. Penalties, hinting at a possible efficiency versus compliance scenario. Conversely, the correlation between risk and penalties is positive, with a value of 0.28, which may indicate that higher risk levels are associated with increased penalties. This relationship underscores the potential cost of risk within operations, where higher risk actions are more likely to result in penalties. Notably, battery usage does not show a strong correlation with any other variable, the strongest being a negative -0.31 with penalties, which might suggest that higher battery usage is not necessarily associated with higher penalties. This could be reflective of operational scenarios where battery usage is independent of the penalty-incurring actions. The subtle correlations between these metrics reflect the complexities of operational dynamics, where each decision or change in one area can have a varied impact on others. Understanding these correlations is essential for informed decision-making, allowing for strategic adjustments that consider the ripple effects across different areas of operation. In addition to the detailed explanation provided, the heatmap in Fig. 9 reveals further nuance. The heatmap in Fig. 9 highlights key relationships between operational metrics: a moderate negative correlation (-0.40) between cost and risk indicates that higher costs are associated with lower risks, suggesting a strategic balance. The negative correlation (-0.45) between time and penalties implies longer operational times reduce penalties, indicating an efficiency-compliance trade-off. A positive correlation (0.28) between risk and penalties shows that higher risks result in increased penalties, emphasizing the financial impact of risky operations.

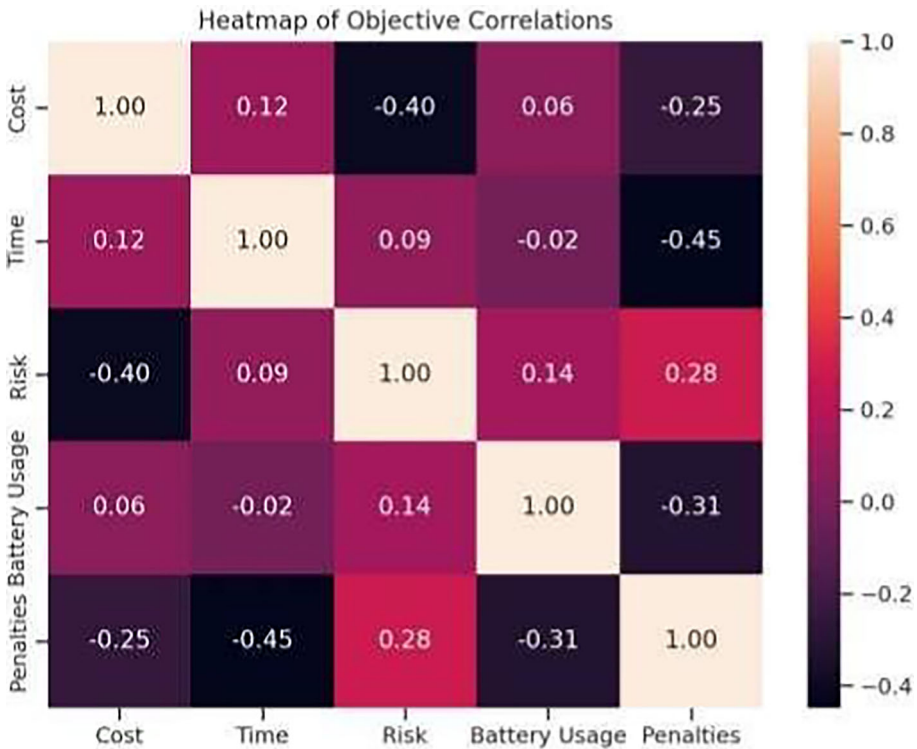


Fig. 9 The heatmap of objectives correlates

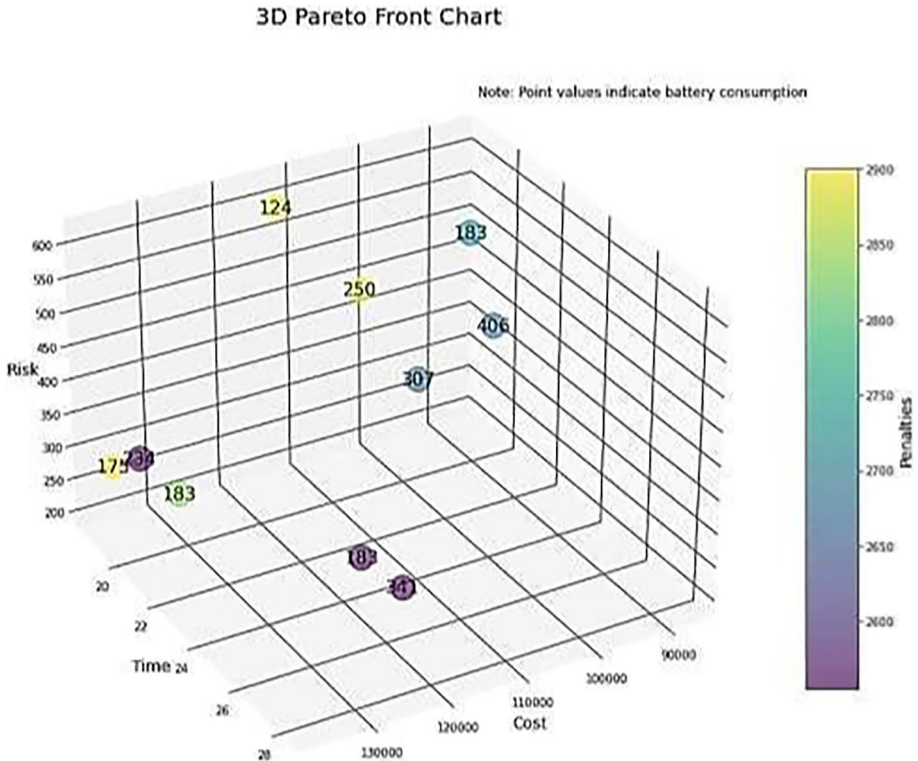


Fig. 10 3D pareto Front of objective functions

5.4.2 3D Pareto Front

The 3D schematic view of Pareto Front Chart in Fig. 10 illustrates the complex interplay between cost, risk, and time, crucial metrics for evaluating performance and efficiency. Observations reveal trade-offs and the extent to which one variable may affect another. Points' positions and colors convey multiple pieces of information, showing that scenarios with minimized risk do not necessarily align with lower costs or penalties. For instance, higher battery usage does not correspond with higher penalties or risk, indicating efficient energy use. This chart helps stakeholders identify areas for improvement by examining the balance of operational metrics.

For instance, points with lower risk values that are closer to the front of the chart represent scenarios with minimized risk. However, these points do not necessarily align with lower costs or penalties, suggesting that reducing risk might come at a higher financial or penal cost. Conversely, points that are higher on the risk axis and closer to the chart's rear suggest scenarios where more time has been taken, potentially to mitigate risk, yet these scenarios do not incur the highest penalties, as indicated by their cooler hues. This might suggest that taking more time—perhaps to ensure thoroughness or compliance—can result in a more favorable balance of risk and penalties, even if the cost is not minimized. Notably, the highest battery usage, indicated by the number 406, does not correspond with the highest penalties or risk, which could imply that higher battery consumption does not necessarily lead to increased

penalties or risk in this operational context. This could be indicative of efficient energy use where increased battery usage is not a sign of inefficiency or elevated risk. The color gradient, reflecting penalties, varies across the spectrum, with the gradient's cooler end representing lower penalties and the warmer end representing higher penalties. The distribution of colors across the chart illustrates that the highest penalties are not exclusively associated with high costs or risks. For instance, a point with a relatively low risk of 250 shows a penalty close to the higher end of the spectrum. This could suggest that penalties in this context are influenced by factors beyond just risk and cost, and perhaps more by operational decisions or externalities not directly captured by the other two metrics. Overall, the 3D Pareto Front Chart is a strategic tool, allowing stakeholders to identify operational efficiencies or deficiencies. By examining the positions and colors of the points in relation to each other, stakeholders can pinpoint areas for potential improvement, such as reducing costs or managing risks more effectively without incurring high penalties. This visualization also opens questions for further analysis, such as the factors contributing to the highest penalties and whether these are within the control of the organization.

5.4.3 Pair plot of pareto front relations

The Fig. 11 presented appears to be a matrix of scatter plots combined with histograms, often referred to as a pair plot, which is a multi-variable analysis tool. This type of visualization enables the simultaneous observation of potential relationships between pairs of variables and the distribution of single variables within the same framework.

The histograms on the diagonal of the matrix offer insights into the distribution of each individual variable: Cost, Time, Risk, Battery Usage, and Penalties. For instance, the histogram for Time suggests a skewed distribution with most occurrences concentrated at lower time values, indicating that most activities occur within a shorter time frame. In contrast, the histogram for Battery Usage indicates a more varied distribution, with several peaks, which may suggest different operational modes or levels of activity. The scatter plots below the diagonal show the relationships between the pairs of variables. For example, the plot at the intersection of Cost and Risk could indicate a potential pattern or trend between these variables, where a cluster of points may suggest a correlation. Similarly, other scatter plots show different concentrations of data points that could suggest varying degrees of association between the variables. The matrix format allows for a comprehensive overview of how each variable interacts with the others, highlighting both the distribution of individual variables and their mutual relationships. This kind of visualization is particularly useful for identifying correlations, outliers, or clusters within the data, which can be pivotal for understanding the complex dynamics of the system from which the data was derived. It also serves as a basis for more detailed statistical analysis, where these visual cues can guide deeper investigations into causality, variance, and other statistical properties. In addition to the comprehensive explanation provided, the figure, a pair plot, further elucidates variable interrelationships and individual distributions:

1. **Histograms:** The diagonal histograms illustrate the distribution of each variable. For instance, "Time" shows a concentration at lower values, indicating most operations are short. "Battery Usage" displays a multimodal distribution, hinting at diverse operational intensities.
2. **Scatter Plots:** The off-diagonal scatter plots reveal potential correlations between variable pairs. For example, the "Cost versus Risk" scatter plot may show a clustering pattern, indicating a possible relationship where specific cost ranges align with certain risk levels.

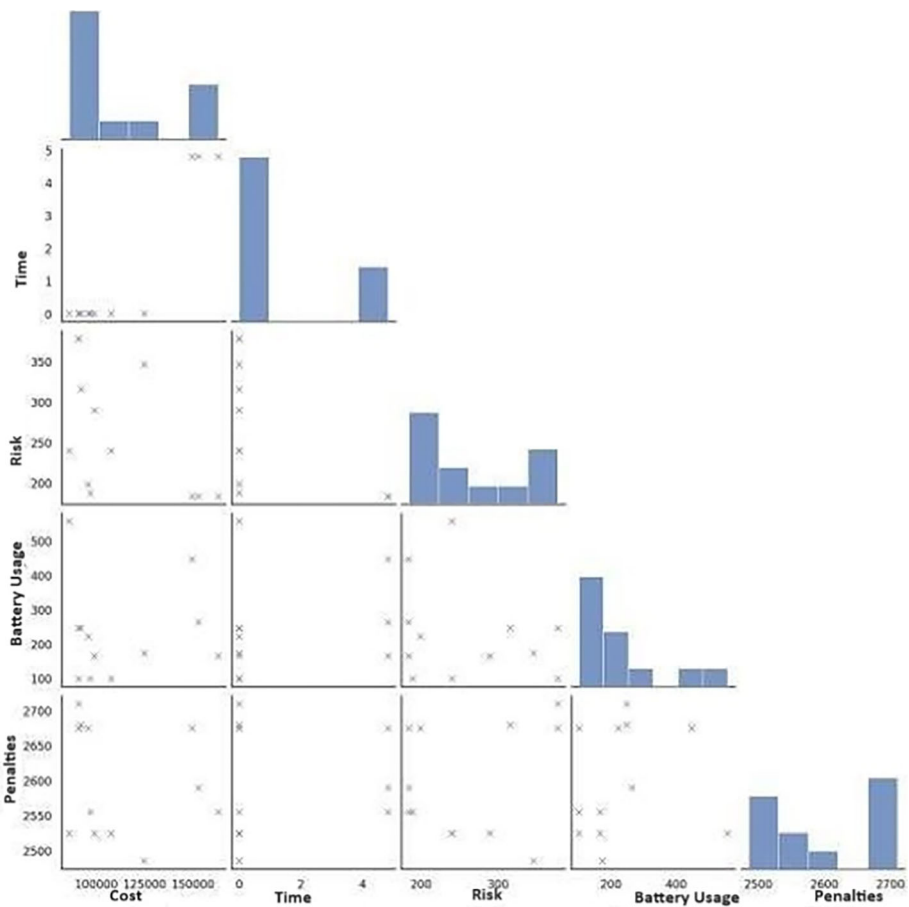


Fig. 11 A matrix of scatter plots of pareto Front Relations

3. **Overall Insights:** This visualization not only identifies individual variable distributions and pairwise relationships but also aids in detecting correlations, outliers, and clusters. It serves as a foundation for deeper statistical analyses, helping to unravel complex system dynamics and guiding targeted investigations into causality and variance.

5.4.4 Bubble chart

The Fig. 12 depicted provides a graphical representation of the relationship between cost and risk, with the additional dimension of penalties indicated by the size of the bubbles. Larger bubbles represent higher penalties, while smaller bubbles represent lower penalties. In this visualization, the distribution of bubbles across the cost-risk plane shows how these two variables correlate, with the variation in bubble size offering insight into the penalty magnitude associated with different cost-risk combinations. The placement of larger bubbles at various points on the chart could suggest that higher penalties are not exclusively occurring at high-risk or high-cost scenarios. Instead, there is a dispersion of penalties across the

range, indicating that high penalties can occur across various levels of cost and risk. The concentration of bubbles in certain areas may point to more common cost-risk scenarios, while sparse areas may indicate less common or outlier situations. If larger bubbles are concentrated in a specific region, it might suggest that higher penalties are more likely in that particular cost and risk range. Conversely, a cluster of smaller bubbles would suggest that those cost and risk combinations are generally associated with lower penalties. The color coding of the bubbles, corresponding to different penalty values, allows for quick visual differentiation between varying levels of penalties. This can be useful for identifying patterns or trends, such as whether there is a trend toward higher penalties with increasing cost or risk. This bubble chart serves as a valuable tool for risk management and financial planning, as it visualizes complex data in an easily interpretable format. By analyzing where the larger bubbles are predominantly located, one can identify which combinations of cost and risk have historically led to higher penalties, and potentially adjust strategies accordingly to mitigate these costs.

5.5 Comparative and evolution analysis

5.5.1 Area chart

The Fig. 13 illustrates the fluctuation of cost, risk, and battery usage over a series of indexed events or time periods. The layers of color represent each variable’s magnitude, stacked to show their cumulative effect at each index point. The cost, represented by the bottommost layer, forms the foundation of the chart, and exhibits significant variation throughout the index, with peaks suggesting instances of high expenditure. The risk layer, while also varying,

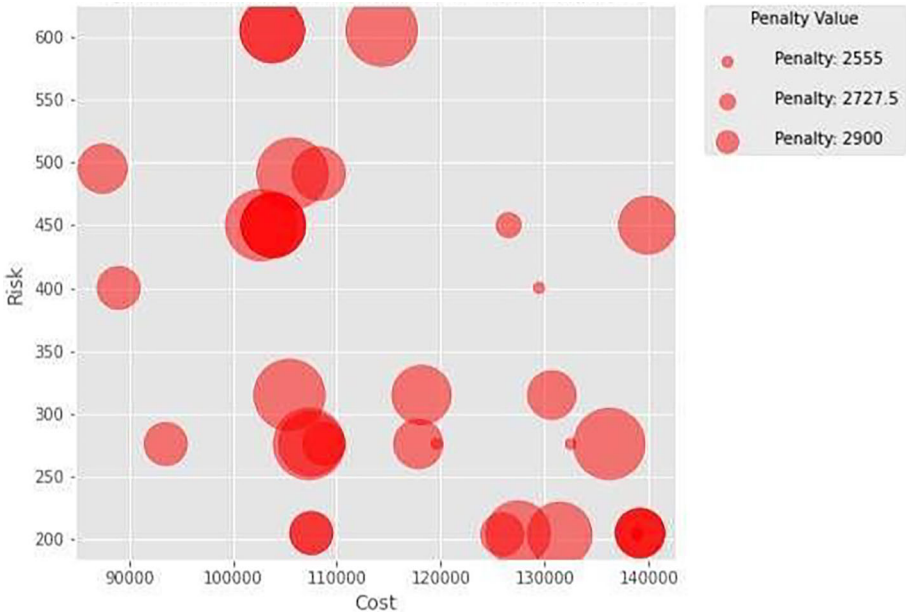


Fig. 12 Bubble chart of cost versus risk

does not seem to correspond directly with the cost's peaks and valleys, indicating that the relationship between cost and risk is not strictly proportional or may be influenced by other factors not depicted in the chart. Above both, the battery usage shows.

spikes that considerably exceed the scale of cost and risk at certain index points. This implies occurrences of high battery consumption, which do not appear to be directly related to the cost or risk levels, suggesting that battery usage is subject to different operational dynamics or constraints. The area chart is a visual representation of the overall trends and can be useful for spotting patterns, such as whether higher costs are typically associated with increased risk or battery usage. However, the overlapping nature of the chart may obscure some of the finer details of these relationships, necessitating a deeper dive into the data for more precise insights. By examining the variability and the relative proportion of each area, one can infer the volatility and impact of each variable within the operational context. Such an analysis might be critical for identifying inefficiencies, forecasting future trends, and allocating resources more effectively.

5.5.2 Network graph

Figure 14 depicts a network graph illustrating the relationship between cost and risk, where the size of each node in the graph represents battery usage. This visual representation allows for an intuitive understanding of how different levels of battery consumption impact the associated costs and risks, facilitating strategic decisions in scenarios where battery management is crucial. The network graph visualizes the interconnectedness of cost and risk with varying node sizes representing battery usage. Each node, likely corresponding to an individual data point or scenario, is connected, indicating potential relationships or dependencies between different cost and risk pairings. The size of each node is indicative of the battery usage associated with each pairing; larger nodes suggest higher battery usage, while smaller nodes indicate lower usage. For example, node 14, being the largest, suggests it is a scenario with substantial battery consumption, possibly an outlier if it significantly deviates from the other node sizes. The thickness of the lines connecting the nodes might suggest the

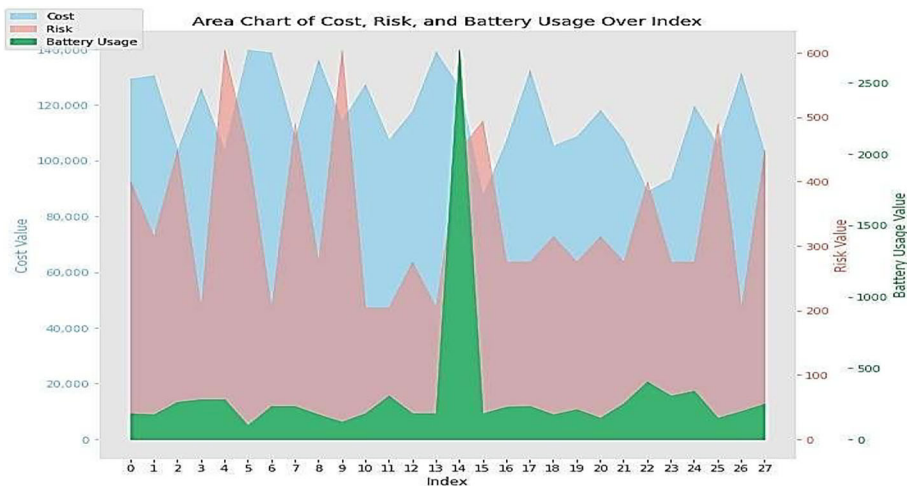


Fig. 13 Area chart of objective functions over index

strength or frequency of the transition between different cost and risk states, or how often certain scenarios occur. If the lines are uniformly thin, this could indicate that transitions between states are not common, or the network is showing a snapshot rather than a process over time. The graph provides an abstract representation that could be used for analyzing operational or system dynamics, especially in contexts where battery usage is a critical factor. The spatial arrangement of nodes can reveal clusters of similar cost-risk scenarios, and the size of nodes within these clusters can indicate which scenarios are most energy-intensive. This visualization can guide strategic decisions, such as identifying which scenarios to target for battery usage reduction or understanding the balance between cost, risk, and energy consumption. By exploring the network, one can discern patterns that might inform policy changes or operational adjustments to enhance efficiency and reduce costs or risks associated with high battery usage.

6 Comparative analysis and validation of optimization results

Before delving into the detailed convergence analysis of the optimization model, it is crucial to understand the role of objective functions in evolutionary algorithms. In optimizing drone routing strategies, the genetic algorithm is precisely configured to enhance a population of potential solutions across multiple dimensions—cost, time, risk, and battery usage. These objective functions act as key metrics, assessing the effectiveness and feasibility of solutions

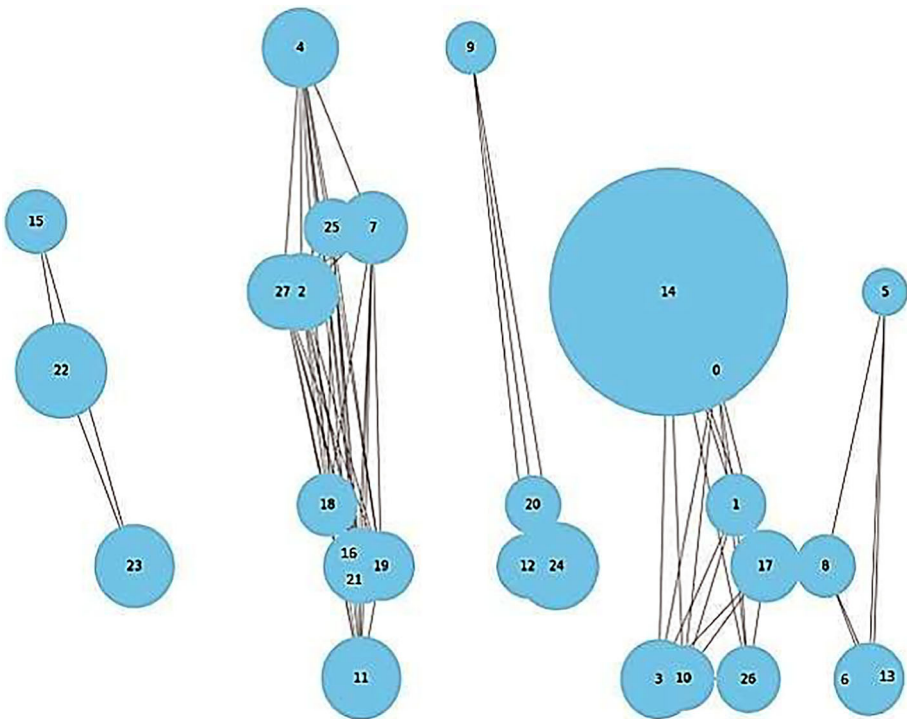


Fig. 14 Network graph of cost versus risk with node size representing battery usage

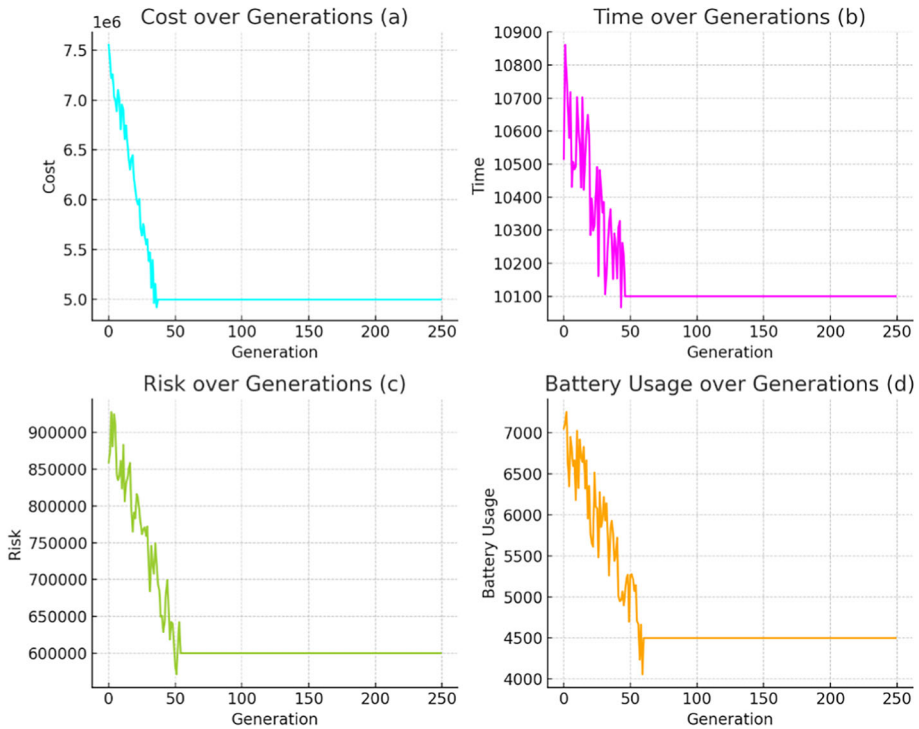


Fig. 15 Visual depiction of the convergence of objective functions over generations: **a** cost, **b** time, **c** risk, **d** battery usage

generated in each iteration. Figure 15, presented next, depicts the convergence behavior of these objective functions, visually demonstrating how the algorithm iteratively focuses on the most promising strategies. It showcases the algorithm's performance across generations, highlighting the evolutionary dynamics that steer the optimization process towards solution stabilization and refinement. This introduction prepares for an in-depth discussion on the algorithm's efficiency, as evidenced by the observed convergence trends in the subsequent charts.

Figure 15 demonstrates the performance of the optimization model over 250 generations, focusing on cost, time, risk, and battery usage. Initially, the genetic algorithm swiftly reduces cost, achieving a stable set of solutions by generation 37. Similarly, time stabilizes by generation 46, risk by generation 54, and battery usage by generation 60. This stepwise improvement pattern indicates that the algorithm quickly identifies near-optimal solutions in the early generations, followed by gradual refinements leading to stability. The results showcase the efficiency and convergence behavior of the algorithm, supported by a population of 300 individuals, with specific probabilities for crossover, mutation, and independence. To better demonstrate the superior performance of the proposed algorithm, a comparison was made with another multi-objective study, specifically Monsef et al. (2019), as shown in the table below which provides a comparison between their method and the current proposed model.

Table 7 provides a comparison between the current proposed model (NSGA-II + BBN) and the method from Monsef et al. (2019), evaluating key criteria such as cost, time, risk,

Table 7 Comparative analysis of optimization performance between the proposed NSGA-II + BBN Model and Monsef et al. (2019)

Criteria	Current Study (NSGA-II + BBN)	Monsef et al. (2019)—NSGA-II
Cost over Generations	Rapid reduction in cost, stabilizing around generation 37 (Figure a)	Slower reduction, stabilizes after 100 generations
Time over Generations	Time stabilizes after 46 generations, faster convergence (Figure b)	Time improves slowly, stabilizing near 200 generations
Risk over Generations	Sharp decrease in risk with stable convergence by 54 generations (Figure c)	No risk assessment is integrated
Battery Usage over Generations	Gradual optimization with fewer oscillations, stabilizing by generation 60 (Figure d)	No Battery usage is integrated
Overall Convergence Rate	Faster convergence in all metrics, achieving stability by 50 generations	Slower convergence, requiring over 100–150 generations for stability
Algorithm Complexity	NSGA-II combined with Bayesian Belief Network (BBN) for risk optimization	NSGA-II without any risk considerations

battery usage, and convergence rate. The proposed model demonstrates superior performance in all these metrics. It achieves faster cost reduction, stabilizing after 37 generations, while Monsef's method requires more than 100 generations. Time stabilization occurs within 46 generations in the proposed model, compared to around 200 generations in Monsef's. Additionally, risk management is a key advantage, utilizing Bayesian Belief Networks (BBN) to reduce risk, a factor absent in Monsef's method. Battery usage is also optimized, stabilizing by generation 60, which is not considered in Monsef et al. (2019). Finally, the proposed model converges faster overall, achieving stability across all metrics within 50 generations, whereas Monsef's approach takes significantly longer to converge. This demonstrates the enhanced efficiency and applicability of the proposed model, particularly in real-world scenarios involving risk and battery management.

7 Conclusion

This study introduces a drone routing optimization model with key insights supported by quantitative analysis, showcasing its potential for enhanced operational efficiency. The model significantly reduced cost and time by averages of 37.3% and 10.48%, respectively, over 250 generations. The NSGAI algorithm effectively optimized drone routing, achieving a cost range of 52–55 million, average time efficiency of 8425, and managing risk levels with an average of 595,108. Box plots and histograms demonstrated the model's adept balance between cost-efficiency and risk management. The correlation heatmap highlighted interdependencies, emphasizing the importance of cost-efficiency and energy management in reducing risks and penalties. The 3D Pareto front and pairplot analyses revealed strategic trade-offs in drone routing optimization. Comparative analysis using area charts and network graphs underscored the model's adept handling of complex routing dynamics. The drone route optimization map indicated strategic placement of the Depot and highlighted varying

visit frequencies at distributors and facilities. The model's classification of scenarios demonstrated adaptability to real-world conditions, emphasizing its potential for future innovations in drone logistics. Future work could involve comparing the proposed model with other optimization algorithms, incorporating additional data sources, or extending the model to other logistics scenarios to explore further improvements and enhance the robustness of drone routing optimization.

Appendix A: Parameters initialization and values assignment

Parameter	Description	Selection Justification
r_i	Point1 = 3; Point2 = 2; Point3 = 5; Point4 = 5; Point5 = 3; Point6 = 3; Point7 = 2; Point8 = 4; Point9 = 4; Point10 = 6; Point11 = 3; Point12 = 2	Selected based on typical delivery demands observed in urban logistics scenarios, reflecting a mix of high and low demand points to ensure diverse test cases
P_i	Point1 = 129; Point2 = 118; Point3 = 149; Point4 = 144; Point5 = 141; Point6 = 150; Point7 = 139; Point8 = 127; Point9 = 121; Point10 = 127; Point11 = 129; Point12 = 129	Values derived from empirical data on population density and commercial activity in urban areas, ensuring realistic representation of demand variability
S_i	('Point1', 'RPA1') = 88; ('Point1', 'RPA2') = 68; ('Point1', 'RPA3') = 50; ('Point1', 'RPA4') = 65; ('Point1', 'RPA5') = 80; ('Point1', 'RPA6') = 79; ('Point1', 'RPA7') = 83; ('Point2', 'RPA1') = 99; ('Point2', 'RPA2') = 98; ('Point2', 'RPA3') = 75; ('Point2', 'RPA4') = 56; ('Point2', 'RPA5') = 69; ('Point2', 'RPA6') = 97; ...	Service times based on historical data and operational efficiency of different drone models, adjusted to simulate a realistic range of scenarios for model testing
Q_k	RPA1 = 200; RPA2 = 250; RPA3 = 150; RPA4 = 150; RPA5 = 200; RPA6 = 150; RPA7 = 150	Capacity values are typical of current commercial drone models used in urban logistics, ensuring practical applicability
a_i	480	Reflects the average starting operational hours for drones in urban settings, based on industry standards

Parameter	Description	Selection Justification
b_i	1020	Maximum operational hours calculated based on battery life and recharge cycles, consistent with manufacturer specifications
M	100,000	Set as a sufficiently large number to act as a constraint in optimization models, ensuring no practical limitations on computational performance
ES_i	Point1 = 3; Point2 = 13; Point3 = 12; Point4 = 15; Point5 = 8; Point6 = 12; Point7 = 14; Point8 = 11; Point9 = 3; Point10 = 13; Point11 = 7; Point12 = 14	Emergency service index based on criticality of each point, derived from historical emergency response data
LS_i	Point1 = 65; Point2 = 70; Point3 = 75; Point4 = 80; Point5 = 60; Point6 = 65; Point7 = 70; Point8 = 75; Point9 = 80; Point10 = 60; Point11 = 65; Point12 = 70	Service level index reflecting customer satisfaction targets, informed by industry benchmarks and best practices
w_2	5	Weight factor chosen to balance cost and efficiency in the optimization model, based on expert judgment
w_3	10	Higher weight given to critical constraints, reflecting their priority in the decision-making process
fix_k	RPA1 = 1000; RPA2 = 1100; RPA3 = 1200; RPA4 = 1300; RPA5 = 1400; RPA6 = 1500; RPA7 = 1600	Fixed costs based on the initial investment and maintenance costs associated with each drone model, ensuring comprehensive cost analysis
C	1.5	Cost of one charging unit based on industry rates for electricity and infrastructure costs
AT	0.42	Minimum charging allowed within the RPA to ensure sufficient operational range, derived from technical specifications of drone batteries

Parameter	Description	Selection Justification
Cf_f	Facility1 = 4.47; Facility2 = 7.62; Facility3 = 4.47; Facility4 = 7.81; Facility5 = 7.81	Preparation costs for facility locations based on construction and operational costs, reflecting industry averages
fix_d	Distributor1 = 250; Distributor2 = 300; Distributor3 = 350; Distributor4 = 400; Distributor5 = 450	Cost of constructing distributor candidate locations based on empirical data from similar logistics projects
DAY	480	Length of a working day in minutes, reflecting typical operational hours for logistics companies
cp_{ji}	('Point1', 'Point1') = 0.0; ('Point1', 'Point2') = 2.3717082451262845; ('Point1', 'Point3') = 2.1213203435596424; ('Point1', 'Point4') = 2.7041634565979917; ('Point1', 'Point5') = 3.0923292192132457; ('Point1', 'Point6') = 3.8242646351945884; ('Point1', 'Point7') = 5.4083269131959835; ('Point1', 'Point8') = 5.7118298293979315; ('Point1', 'Point9') = 7.5; ('Point1', 'Point10') = 7.721722605740251; ...	Battery consumption between nodes based on the Euclidean distance and drone power consumption rates, ensuring realistic energy usage modeling
dx_{ij}	('Point1', 'Point2') = 15.81; ('Point1', 'Point3') = 14.14; ('Point1', 'Point4') = 18.03; ('Point1', 'Point5') = 20.62; ('Point1', 'Point6') = 25.5; ('Point1', 'Point7') = 36.06; ('Point1', 'Point8') = 38.08; ('Point1', 'Point9') = 50.0; ('Point1', 'Point10') = 51.48; ('Point1', 'Point11') = 50.0; ('Point1', 'Point12') = 55.9; ('Point2', 'Point1') = 15.81; ('Point2', 'Point3') = 25.5; ('Point2', 'Point4') = 11.18; ...	Distances between nodes calculated using geographical data, ensuring accurate routing and distance-based constraints

Parameter	Description	Selection Justification
p_u	Scenario1 = 0.33; Scenario2 = 0.33; Scenario3 = 0.34	Probabilities of scenarios based on expert analysis and historical data, ensuring diverse and realistic scenario testing
V_{ku}	RPA1 = {'Scenario1': 110, 'Scenario2': 120, 'Scenario3': 130}; RPA2 = {'Scenario1': 110, 'Scenario2': 120, 'Scenario3': 130}; RPA3 = {'Scenario1': 110, 'Scenario2': 120, 'Scenario3': 130}; RPA4 = {'Scenario1': 110, 'Scenario2': 120, 'Scenario3': 130}; ...	Velocity of RPAs in different scenarios based on drone performance data and operational conditions
cap_d	Distributor1 = 845; Distributor2 = 866; Distributor3 = 871; Distributor4 = 884; Distributor5 = 838	Capacities of distributor locations based on storage and operational limits, reflecting typical logistics hub capacities
\overline{cap}_f	Facility1 = 140; Facility2 = 150; Facility3 = 145; Facility4 = 143; Facility5 = 120	Facility capacities derived from industry standards for operational hubs, ensuring practical constraints
$L0_k$	RPA1 = 784; RPA2 = 849; RPA3 = 794; RPA4 = 849; RPA5 = 847; RPA6 = 781; RPA7 = 854	Initial load on RPAs when leaving the distributor based on typical payloads and drone capacities
S_{ij}^k	('RPA1', 'Point1', 'Point1') = 0; ('RPA1', 'Point1', 'Point2') = 500; ('RPA1', 'Point1', 'Point3') = 600; ('RPA1', 'Point1', 'Point4') = 200; ('RPA1', 'Point1', 'Point5') = 300; ('RPA1', 'Point1', 'Point6') = 500; ('RPA1', 'Point1', 'Point7') = 300; ('RPA1', 'Point1', 'Point8') = 600; ('RPA1', 'Point1', 'Point9') = 500; ('RPA1', 'Point1', 'Point10') = 600; ('RPA1', 'Point1', 'Point11') = 500; ('RPA1', 'Point1', 'Point12') = 500; ...	Risk of route derived from node i to node j with RPA k, based on BBN risk assessment methodology

Parameter	Description	Selection Justification
s_{iu}	Point1 = {'Scenario1': 45, 'Scenario2': 36, 'Scenario3': 37}; Point2 = {'Scenario1': 33, 'Scenario2': 34, 'Scenario3': 37}; Point3 = {'Scenario1': 47, 'Scenario2': 41, 'Scenario3': 31}; Point4 = {'Scenario1': 38, 'Scenario2': 44, 'Scenario3': 36}; ...	Time to start providing service to demand point i in scenario u , based on operational schedules and scenario analysis
L_j	Point1 = 25; Point2 = 36; Point3 = 30; Point4 = 35; Point5 = 28; Point6 = 30; Point7 = 20; Point8 = 28; Point9 = 39; Point10 = 37; Point11 = 38; Point12 = 32	Load weight remaining on the RPA after service to demand point j , derived from payload capacities and operational constraints
E_{iu}	('Point1', 'Scenario1') = 23; ('Point1', 'Scenario2') = 23; ('Point1', 'Scenario3') = 23; ('Point2', 'Scenario1') = 26; ('Point2', 'Scenario2') = 26; ('Point2', 'Scenario3') = 26; ('Point3', 'Scenario1') = 20; ('Point3', 'Scenario2') = 20; ('Point3', 'Scenario3') = 20; ('Point4', 'Scenario1') = 23; ('Point4', 'Scenario2') = 23; ('Point4', 'Scenario3') = 23; ('Point5', 'Scenario1') = 26; ('Point5', 'Scenario2') = 26; ...	Time deviation from the earliest time allowed to provide service to demand point i in the soft time window in scenario u , based on scheduling flexibility
L_{iu}	('Point1', 'Scenario1') = 40; ('Point1', 'Scenario2') = 40; ('Point1', 'Scenario3') = 40; ('Point2', 'Scenario1') = 45; ('Point2', 'Scenario2') = 45; ('Point2', 'Scenario3') = 45; ('Point3', 'Scenario1') = 35; ('Point3', 'Scenario2') = 35; ('Point3', 'Scenario3') = 35; ('Point4', 'Scenario1') = 40; ('Point4', 'Scenario2') = 40; ('Point4', 'Scenario3') = 40; ('Point5', 'Scenario1') = 45; ('Point5', 'Scenario2') = 45; ...	Time deviation from the latest time allowed to provide service to demand point i in the soft time window in scenario u , reflecting possible delays
α	0.5	Parameter for scaling deviations, set to balance early and late service penalties

Parameter	Description	Selection Justification
β	0.7	Parameter for scaling deviations, set to emphasize the importance of late service penalties
FC_k	RPA1 = 700; RPA2 = 720; RPA3 = 740; RPA4 = 760; RPA5 = 780; RPA6 = 800; RPA7 = 820	Reflects fixed costs (maintenance, depreciation, etc.). Values increase incrementally to represent differences in drone capabilities and usage, based on operational data
de_d	Distributor1 = 89; Distributor2 = 75; Distributor3 = 74; Distributor4 = 90; Distributor5 = 97	Center demand of distributor d based on historical demand data and operational capacity
A_i	0.42 for all drones	Amount of battery available on the RPA, based on manufacturer specifications and operational needs
C_{ij}^k	('Point1', 'Point1') = 0; ('Point1', 'Point2') = 7; ('Point1', 'Point3') = 6; ('Point1', 'Point4') = 9; ('Point1', 'Point5') = 4; ...	Energy consumption by a drone of type k to fly from i to j, based on distance and drone power consumption rates
C_k	RPA1 = 160; RPA2 = 170; RPA3 = 180; RPA4 = 190; RPA5 = 200; RPA6 = 210; RPA7 = 220	Amortized cost of the drone type k, based on purchase price and maintenance costs spread over operational life
C_{bat}^k	RPA1 = 23; RPA2 = 26; RPA3 = 29; RPA4 = 32; RPA5 = 35; RPA6 = 38; RPA7 = 41	Amortized cost of the battery of drone type k, reflecting replacement and maintenance costs
C_E	0.1	Cost per unit of energy, derived from industry rates for electricity
C_L	30	Wage of drone operators, based on industry standards for labor costs
n_k	2	Number of drones of type k a drone operator can operate, based on industry standards and operational efficiency
C_k^M	RPA1 = 100; RPA2 = 105; RPA3 = 110; RPA4 = 115; RPA5 = 120; RPA6 = 125; RPA7 = 130	Maintenance cost of a drone of type k, reflecting routine maintenance and repair costs

Parameter	Description	Selection Justification
t_k^{bat}	20 for all drones	Time required to replace the battery of drone type k, based on manufacturer specifications and operational procedures
l_i	Point1 = 15; Point2 = 19; Point3 = 20; Point4 = 17; Point5 = 27; Point6 = 33; Point7 = 30; Point8 = 17; Point9 = 17; Point10 = 28; Point11 = 20; Point12 = 20	Distance of delivery location i from depot, based on geographical data and routing plans
l_j	Point1 = 17; Point2 = 12; Point3 = 25; Point4 = 21; Point5 = 16; Point6 = 10; Point7 = 18; Point8 = 24; Point9 = 24; Point10 = 24; Point11 = 18; Point12 = 17	Distance of delivery location j from depot, reflecting typical urban logistics distances
t_{ij}	('Point1', 'Point1') = 0; ('Point1', 'Point2') = 8; ('Point1', 'Point3') = 15; ('Point1', 'Point4') = 8; ('Point1', 'Point5') = 13; ('Point1', 'Point6') = 14; ('Point1', 'Point7') = 5; ('Point1', 'Point8') = 5; ('Point1', 'Point9') = 13; ('Point1', 'Point10') = 13; ('Point1', 'Point11') = 6; ('Point1', 'Point12') = 6; ('Point2', 'Point1') = 14; ('Point2', 'Point2') = 0; ('Point2', 'Point3') = 6; ...	Time required for drone to arrive at delivery location from i to j, based on operational speeds and distances
e_i	Point1 = 7; Point2 = 7; Point3 = 7; Point4 = 9; Point5 = 8; Point6 = 7; Point7 = 8; Point8 = 9; Point9 = 7; Point10 = 8; Point11 = 9; Point12 = 9	Earliest possible pickup time, based on operational schedules and demand patterns
ch_k^o	90 for all drones	Initial energy in the battery of drone type k, reflecting full charge capacity
ch_k^{min}	20 for all drones	Minimum remaining energy required in the battery of drone type k, ensuring sufficient power for return or emergency landing

Parameter	Description	Selection Justification
ch_k^{max}	80 for all drones	Maximum remaining energy required in the battery of drone type k, reflecting battery capacity limits, set lower than full capacity to ensure operational safety and longevity
Δch_j	Point1 = 0.36; Point2 = 0.47; Point3 = 0.25; Point4 = 0.16 Point5 = 0.23; Point6 = 0.18; Point7 = 0.45; Point8 = 0.20; Point9 = 0.36; Point10 = 0.21; Point11 = 0.24; Point12 = 0.44	Maximum permissible delay for point j, based on operational constraints and delivery urgency
M_k^{max}	RPA1 = 70; RPA2 = 80; RPA3 = 90; RPA4 = 100; RPA5 = 110; RPA6 = 120; RPA7 = 130	Maximum package weight carrying capacity of drone type k, based on manufacturer specifications
M_i	Point1 = 5; Point2 = 4; Point3 = 5; Point4 = 4; Point5 = 5; Point6 = 4; Point7 = 3; Point8 = 2; Point9 = 4; Point10 = 3; Point11 = 5; Point12 = 4	Package weight for delivery location i, based on typical delivery items in urban logistics
Constraint Penalties	constraint_5_penalty = 300 # Each demand point covered at least once constraint_6_penalty = 250 # In-flow and out-flow balance constraint_7_penalty = 200 # Drone utilization constraint_8_penalty = 150 # Avoiding self-routing : : constraint_57_penalty = 200 # Time Condition Waiting Feasibility constraint_58_penalty = 150 # g_i and Δch_j Relation	Penalties set based on the severity of constraint violations, ensuring appropriate weighting in the optimization model to prioritize critical operational constraints

Appendix B: Tale B1: Description of Numerical Labels in Fig. 14

Node	Description
0	Scenario with the highest battery usage, indicating substantial consumption
1	Low cost, moderate risk scenario
2	Moderate cost, moderate risk scenario
3	Low cost, low risk scenario
4	High cost, low risk scenario
5	Low cost, high risk scenario
6	Moderate cost, low risk scenario
7	Moderate cost, high risk scenario
8	Low cost, high battery usage scenario
9	High cost, high risk scenario
10	Low cost, moderate risk scenario
11	High battery usage, moderate cost scenario
12	Moderate battery usage, low cost scenario
13	High risk, low cost scenario
14	Scenario with the highest cost and risk
15	Low battery usage, high cost scenario
16	Moderate cost, high battery usage scenario
17	Low risk, low cost scenario
18	High risk, high battery usage scenario
19	Moderate risk, moderate battery usage scenario
20	Low battery usage, low risk scenario
21	High battery usage, moderate risk scenario
22	High cost, low battery usage scenario
23	Low cost, low battery usage scenario
24	Moderate cost, low battery usage scenario
25	Moderate cost, high risk scenario
26	Low battery usage, moderate risk scenario
27	Moderate battery usage, high cost scenario

Funding No funds, grants, or other support was received.

Declarations

Conflict of interest Armin Mahmoodi declares that he has no conflict of interest. Seyed Mojtaba Sajadi declares that he has no conflict of interest. Abdellatif M. Sadeq declares that he has no conflict of interest. Masoud

Narenji declares that he has no conflict of interest. Mehdi Eshaghi declares that he has no conflict of interest. Milad Jasemi declares that he has no conflict of interest.

Ethical approval This article does not contain any studies with human participants performed by any of the authors.

Informed consent Informed consent was obtained from all individual participants included in the study.

Open Access This article is licensed under a Creative Commons Attribution 4.0 International License, which permits use, sharing, adaptation, distribution and reproduction in any medium or format, as long as you give appropriate credit to the original author(s) and the source, provide a link to the Creative Commons licence, and indicate if changes were made. The images or other third party material in this article are included in the article's Creative Commons licence, unless indicated otherwise in a credit line to the material. If material is not included in the article's Creative Commons licence and your intended use is not permitted by statutory regulation or exceeds the permitted use, you will need to obtain permission directly from the copyright holder. To view a copy of this licence, visit <http://creativecommons.org/licenses/by/4.0/>.

References

- Allouch, A., Koubaa, A., Khalgui, M., & Abbes, T. (2019). Qualitative and quantitative risk analysis and safety assessment of unmanned aerial vehicles missions over the internet. *Ieee Access*, 7, 53392–53410.
- Arishi, A., Krishnan, K., & Arishi, M. (2022). Machine learning approach for truck-drones based last-mile delivery in the era of industry 4.0. *Engineering Applications of Artificial Intelligence*, 116, 105439.
- Balador, A., Kouba, A., Cassioli, D., Foukalas, F., Severino, R., Stepanova, D., ... & Sukuvaara, T. (2018). Wireless communication technologies for safe cooperative cyber physical systems. *Sensors*, 18(11), 4075.
- Baubion, C. (2013). OECD risk management: Strategic crisis management. *OECD Working Papers on Public Governance*, 23, 9–21.
- Bareither, C., & Luxhøj, J. T. (2007). Uncertainty and sensitivity analysis in bayesian belief networks: Applications to aviation safety risk assessment. *International Journal of Industrial and Systems Engineering*, 2(2), 137–158.
- Bhuiyan, T. H., Roni, M., & Walker, V. (2022). RPAS deployment optimization for direct delivery with time windows and battery replacements. In *RPAS conference, Optimization and Control* (math.OC). [arXiv:2209.04057](https://arxiv.org/abs/2209.04057). <https://doi.org/10.48550/arXiv.2209.04057>.
- Bi, Z., Guo, X., Wang, J., Qin, S., & Liu, G. (2023). Deep reinforcement learning for truck-drone delivery problem. *Drones*, 7, 445.
- Bi, Z., Guo, X., Wang, J., Qin, S., & Liu, G. (2024). Truck-Drone delivery optimization based on multi-agent reinforcement learning. *Drones*, 8, 27. <https://doi.org/10.3390/drones8010027>
- Chang, J., & Laliberte, J. (2023). Trajectory optimization for dynamic soaring remotely piloted aircraft with under-wing solar panels. *Journal of Aircraft*. <https://doi.org/10.2514/1.C037105>
- Chauhan, D. R., Unnikrishnan, A., Figliozzi, M., & Boyles, S. D. (2020). Robust maximum coverage facility location problem with drones considering uncertainties in battery availability and consumption. *Transportation Research Record*.
- Chauhan, D., Unnikrishnan, A., & Figliozzi, M. (2019). Maximum coverage capacitated facility location problem with range constrained RPASs. *Transportation Research Part C: Emerging Technologies*, 99, 1–18. <https://doi.org/10.1016/j.trc.2018.12.001>
- Cheng, C., Adulyasak, Y., & Rousseau, L.-M. (2020). Drone routing with energy function: Formulation and exact algorithm. *Transportation Research Part b: Methodological*, 139, 364–387. <https://doi.org/10.1016/j.trb.2020.06.011>
- Chi, N. T. K., Phong, L. T., & Hanh, N. T. (2023). The drone delivery services: An innovative application in an emerging economy. *The Asian Journal of Shipping and Logistics*, 39(2), 39–45. <https://doi.org/10.1016/j.ajsl.2023.01.002>
- Chiang, W.-C., Li, Y., Shang, J., & Urban, T. L. (2019). Impact of drone delivery on sustainability and cost: Realizing the UAV potential through vehicle routing optimization. *Applied Energy*, 242, 1164–1175. <https://doi.org/10.1016/j.apenergy.2019.03.117>
- Choi, Y., & Schonfeld, P. M. (2017). Optimization of multi-package RPAS deliveries considering battery capacity. In *Proceedings of the 96th annual meeting of the transportation research board*, Washington, DC, USA (pp. 8–12). <https://trid.trb.org/view/1439294>

- Chouzenoux, É., & Elvira, V. (2024). Graphical inference in non-Markovian linear-Gaussian state-space mod1120 els. In ICASSP 2024–2024 IEEE international conference on acoustics, speech and signal processing 1121 (ICASSP), Seoul, Republic of Korea (pp. 13141–13145). <https://doi.org/10.1109/ICASSP48485.2024>
- Chung, S. H., Sah, B., & Lee, J. (2020). Optimization for drone and drone-truck combined operations: A review of the state of the art and future directions. *Computers & Operations Research*, *123*, 105004. <https://doi.org/10.1016/j.cor.2020.105004>
- Coelho, B. N., Coelho, V. N., Coelho, I. M., Ochi, L. S., Koochaksaraei, R.H., Zuidema, D., Lima, M. S. F., & da Costa, A. R. (2017). A multi-objective green UAV routing problem. *Computers & Operations Research*, *88*, 306–315. <https://doi.org/10.1016/j.cor.2017.04.011>
- Das, A. K., Marks, R. J., El-Sharkawi, M., Arabshahi, P., & Gray, A. (2004, November). Optimization methods for minimum power bidirectional topology construction in wireless networks with sectored antennas. In *IEEE Global Telecommunications Conference*, 2004. GLOBECOM'04. (Vol. 6, pp. 3962–3968). IEEE.
- Das, B., Mukherjee, V., & Das, D. (2020). Student psychology based optimization algorithm: A new population based optimization algorithm for solving optimization problems. *Advances in Engineering software*, *146*, 102804.
- Dell'Amico, M., Montemanni, R., & Novellani, S. (2022). Exact models for the flying sidekick traveling salesman problem. *International Transactions in Operational Research*, *29*(3), 1360–1393. <https://doi.org/10.1111/itor.13030>
- Dorling, K., Heinrichs, J., Messier, G. G., & Magierowski, S. (2017). Vehicle routing problems for drone delivery. *IEEE Transactions on Systems, Man, and Cybernetics: Systems*, *47*(1), 70–85. <https://doi.org/10.1109/TSMC.2016.2582745>
- Elvira, V., & Chouzenoux, É. (2022). Graphical inference in linear-Gaussian state-space models. *IEEE Transactions on Signal Processing*, *70*, 4757–4771. <https://doi.org/10.1109/TSP.2022.3209016>
- Erkut, E., & Ingolfsson, A. (2005). Transport risk models for hazardous materials: revisited (January 1, 2004). *Operations Research Letters* *33*(1), 81–89. University of Alberta School of Business Research Paper No. 2013–180, Available at SSRN: <https://ssrn.com/abstract=2274774>
- Eskandaripour, H., & Boldsaiikhan, E. (2023). Last-Mile drone delivery: Past, present, and future. *Drones*, *7*, 77. <https://doi.org/10.3390/drones7020077>
- Figliozzi, M. A. (2017). Lifecycle modeling and assessment of unmanned aerial vehicles (RPASs) co2e emissions. *Transportation Research Part D: Transport and Environment*, *57*, 251–261. <https://doi.org/10.1016/j.trd.2017.09.011>
- Freitas, J. C., Penna, P. H. V., & Toffolo, T. A. (2022). Exact and heuristic approaches to Truck-Drone delivery problems. *EURO Journal on Transportation and Logistics*, *12*, 100094.
- Gohari, A., Ahmad, A. B., Rahim, R. B. A., Supa'at, A., Abd Razak, S., & Gismalla, M. S. M. (2022). Involvement of surveillance drones in smart cities: A systematic review. *IEEE Access*, *10*, 56611–56628.
- Guo, X., Bi, Z., Wang, J., Qin, S., Liu, S., & Qi, L. (2023). Reinforcement learning for disassembly system optimization problems: A survey. *Int. J. Netw. Dyn. Intell.*, *2*, 1–14.
- Ha, Q. M., Deville, Y., Pham, Q. D., & Hà, M. H. (2018). On the mincost traveling salesman problem with RPAS. *Transportation Research Part C: Emerging Technologies*, *86*, 597–621. <https://doi.org/10.1016/j.trc.2017.11.015>
- Han, Y., Liu, L., Duan, L., & Zhang, R. (2020). Towards reliable UAV swarm communication in D2D-enhanced cellular networks. *IEEE Transactions on Wireless Communications*, *20*(3), 1567–1581.
- Han, Y., Liu, H., Wang, Y., & Liu, C. (2022). A comprehensive review for typical applications based upon unmanned aerial vehicle platform. *IEEE Journal of Selected Topics in Applied Earth Observations and Remote Sensing*, *15*, 9654–9666.
- Hashemi, L., Mahmoodi, A., Jasemi, M., Millar, R. C., & Laliberté, J. (2021). Modeling a robust multi-objective locating-routing problem with bounded delivery time using meta-heuristic algorithms. *Smart and Resilient Transportation*, *3*(3), 283–303. <https://doi.org/10.1108/SRT-08-2021-0008>
- Hashemi, L., Mahmoodi, A., Jasemi, M., Millar, R. C., & Laliberté, J. (2022). Designing a locating-routing three-echelon supply chain network under uncertainty. *International Journal of Intelligent Computing and Cybernetics*, *15*(4), 562–588. <https://doi.org/10.1108/IJICC-08-2021-0163>
- Hu, X., Pang, B., Dai, F., & Low, K. H. (2020). Risk assessment model for UAV cost-effective path planning in urban environments. *IEEE Access*, *8*, 150162–150173.
- Janik, P., Zawistowski, M., Fellner, R., & Zawistowski, G. (2021). Unmanned aircraft systems risk assessment based on SORA for first responders and disaster management. *Applied Sciences*, *11*, 5364. <https://doi.org/10.3390/app11125364>
- Jiao, Q., Liu, Y., Zheng, Z., Sun, L., Bai, Y., Zhang, Z., Sun, L., Ren, G., Zhou, G., Chen, X., et al. (2022). Ground risk assessment for unmanned aircraft systems based on dynamic model. *Rpass*, *6*, 324. <https://doi.org/10.3390/RPASs6110324>


- Jiao, X., Chen, J., Jiang, K., Cao, Z., & Yang, D. (2023). Autonomous driving risk assessment with boundary-based environment model. *IEEE Transactions on Intelligent Vehicles*, 9(1), 642–655.
- Kevorkian, C. G. (2016). UAS risk analysis using Bayesian belief networks: An application to the Virginia Tech ESPAARO Master Thesis. Faculty of the Virginia Polytechnic Institute and State University. pp. 24–56.
- Kishk, M. A., Bader, A., & Alouini, M. S. (2020). On the 3-D placement of airborne base stations using tethered UAVs. *IEEE Transactions on Communications*, 68(8), 5202–5215.
- Kong, F., Li, J., Jiang, B., Wang, H., & Song, H. (2023). Trajectory optimization for drone logistics delivery via attention-based pointer network. *IEEE Transactions on Intelligent Transportation Systems*, 24(4), 4519–4531. <https://doi.org/10.1109/TITS.2022.3168987>
- Kumbhar, F. H., & Shin, S. Y. (2022). Novel vehicular compatibility-based ad hoc message routing scheme in the internet of vehicles using machine learning. *IEEE Internet of Things Journal*, 9(4), 2817–2828. <https://doi.org/10.1109/JIOT.2021.3093545>
- Kyriakakis, N. A., Aronis, S., Marinaki, M., & Marinakis, Y. (2023). A GRASP/VND algorithm for the energy minimizing drone routing problem with pickups and deliveries. *Computers & Industrial Engineering*, 182, 109340.
- Li, H., Chen, J., Wang, F., & Bai, M. (2021). Ground-vehicle and unmanned-aerial-vehicle routing problems from two-echelon scheme perspective: A review. *European Journal of Operational Research*, 294(3), 1078–1095. <https://doi.org/10.1016/j.ejor.2021.02.022>
- Liang, Y., & Kelemen, A. (2016). Bayesian state space models for dynamic genetic network construction across multiple tissues. *Statistical Applications in Genetics and Molecular Biology*, 15(4), 273–290. <https://doi.org/10.1515/sagmb-2014-0055>
- Liu, Y., Liu, Z., Shi, J., Wu, G., & Pedrycz, W. (2021). Two-echelon routing problem for parcel delivery by cooperated truck and drone. *IEEE Transactions on Systems, Man, and Cybernetics: Systems*, 51(12), 7450–7465. <https://doi.org/10.1109/TSMC.2020.2968839>
- Liu, Z., Li, X., & Khojandi, A. (2022). The flying sidekick traveling salesman problem with stochastic travel time: A reinforcement learning approach. *Transportation Research Part e: Logistics and Transportation Review*, 164, 102816.
- Luo, Z., Poon, M., Zhang, Z., Liu, Z., & Lim, A. (2021a). The multi-visit traveling salesman problem with multi-drones. *Transportation Research Part c: Emerging Technologies*, 128, 103172. <https://doi.org/10.1016/j.trc.2021.103172>
- Luo, Z., Poon, M., Zhang, Z., Liu, Z., & Lim, A. (2021b). The multi-visit traveling salesman problem with multi-RPASs. *Transportation Research Part C: Emerging Technologies*, 128, 103172. <https://doi.org/10.1016/j.trc.2021.103172>
- Macrina, G., Di Puglia Pugliese, L., Guerriero, F., & Laporte, G. (2020). Drone-aided routing: A literature review. *Transportation Research Part C: Emerging Technologies*, 120, 102762. <https://doi.org/10.1016/j.trc.2020.102762>
- Mahmoodi, A., & Hashemi, L. (2024). Strategic justification of integrated resource planning tools in organizations. *Business Process Management Journal*. <https://doi.org/10.1108/BPMJ-11-2023-0902>
- Mahmoodi, A., Hashemi, L., Laliberté, J., & Millar, R. C. (2022). Secured multi-dimensional robust optimization model for remotely piloted aircraft system (RPAS) delivery network based on the SORA standard. *Designs*, 6, 55. <https://doi.org/10.3390/designs6030055>
- Mahmoodi, A., Hashemi, L., Laliberté, J., Millar, R. C., & Meyer, R. W. (2024). Revolutionizing RPAS logistics and reducing CO2 emissions with advanced RPAS technology for delivery systems. *Cleaner Logistics and Supply Chain*, 12, 100166. <https://doi.org/10.1016/j.clscn.2024.100166>
- Millar, R. C. (2015). A multifaceted investigation and intervention into the process of flight clearance for UAS experimental flight test. *SAE International Journal of Aerospace*, 8(2), 183–188.
- Millar, R. C., Hashemi, L., Mahmoodi, A., Meyer, R. W., & Laliberté, J. (2023). Integrating unmanned and manned RPAS data network based on combined Bayesian belief network and multi-objective reinforcement learning algorithm. *Drone Systems and Applications*, 11, 1–17. <https://doi.org/10.1139/dsa-2022-0043>
- Monsef, H., Naghashzadegan, M., Jamali, A., & Farmani, R. (2019). Comparison of evolutionary multi objective optimization algorithms in optimum design of distribution network. *Ain Shams Engineering Journal*, 10(1), 103–111. <https://doi.org/10.1016/j.asej.2018.04.003>
- Mulumba, T., & Diabat, A. (2024). Optimization of the RPA-assisted pickup and delivery problem. *Transportation Research Part e: Logistics and Transportation Review*, 181, 103377. <https://doi.org/10.1016/j.trc.2023.103377>
- Mulvey, J. M., Vanderbei, R. J., & Zenios, S. A. (1995). Robust optimization of large-scale systems. *Operations Research*, 43(2), 264–281.

- Murray, C. C., & Chu, A. G. (2015). The flying sidekick traveling salesman problem: Optimization of drone-assisted parcel delivery. *Transportation Research Part c: Emerging Technologies*, 54, 86–109. <https://doi.org/10.1016/j.trc.2015.03.005>
- Nagakura, D. (2019). Computing exact score vectors for linear Gaussian state space models. *Communications in Statistics - Simulation and Computation*, 50(8), 2313–2326. <https://doi.org/10.1080/03610918.2019.1601216>
- Nguyen, K. V., Nguyen, C. H., Van Do, T., & Rotter, C. (2023). Efficient multi-UAV assisted data gathering schemes for maximizing the operation time of wireless sensor networks in precision farming. *IEEE Transactions on Industrial Informatics*, 19(12), 11664–11674.
- Nguyen, M. A., Dang, G. T. H., Hà, M. H., & Pham, M. T. (2022). The min-cost parallel drone scheduling vehicle routing problem. *European J. Oper. Res.*, 299(3), 910–930.
- Ning, C., & You, F. (2019). Optimization under uncertainty in the era of big data and deep learning: When machine learning meets mathematical programming. *Computers & Chemical Engineering*, 125, 434–448. <https://doi.org/10.1016/j.compchemeng.2019.03.034>
- Rabta, B., Wankmüller, C., & Reiner, G. (2018). A drone fleet model for last-mile distribution in disaster relief operations. *International Journal of Disaster Risk Reduction*, 28, 107–112. <https://doi.org/10.1016/j.ijdrr.2018.02.020>
- Rojas Viloria, D., Solano-Charris, E. L., Muñoz-Villamizar, A., & Montoya-Torres, J. R. (2021). Unmanned aerial vehicles/drones in vehicle routing problems: A literature review. *International Transactions in Operational Research*, 28(4), 1626–1657. <https://doi.org/10.1111/itor.12783>
- Roweis, S., & Ghahramani, Z. (1999). A unifying review of linear Gaussian models. *Neural Computation*, 11(2), 305–345. <https://doi.org/10.1162/089976699300016674>
- Sajid, M., Mittal, H., Pare, S., & Prasad, M. (2022). Routing and scheduling optimization for UAV assisted delivery system: A hybrid approach. *Applied Soft Computing*, 126, 109225.
- San, K. T., Lee, E. Y., Chang, Y. S. (2016) The delivery assignment solution for swarms of UAVs dealing with multi-dimensional chromosome representation of genetic algorithm. In *2016 IEEE 7th annual ubiquitous computing, electronics & mobile communication conference (UEMCON)*, New York, NY, USA (pp. 1–7). <https://doi.org/10.1109/UEMCON.2016.7777839>
- Sham, R., Chong, H. X., Aw, E.C.-X., Thangal, T. B. T., & binti Abdamia, N. (2023). Switching up the delivery game: Understanding switching intention to retail drone delivery services. *Journal of Retailing and Consumer Services*, 75, 103478. <https://doi.org/10.1016/j.jretconser.2023.103478>
- Shen, Z. M., & Sun, Y. (2023). Strengthening supply chain resilience during COVID-19: A case study of JD.com. *Journal of Operations Management*, 69(3), 359–383.
- Song, B. D., Park, K., & Kim, J. (2018). Persistent UAV delivery logistics: MILP formulation and efficient heuristic. *Computers & Industrial Engineering*, 120, 418–428. <https://doi.org/10.1016/j.cie.2018.05.013>
- JARUS Guidelines on Specific Operations Risk Assessment (SORA). (2021). Available online: http://jarus-rpas.org/sites/jaruspas.org/files/jar_doc_06_jarus_sora_v2.0.pdf. Accessed on 15 April 2022.
- Torabbeigi, M., Lim, G. J., & Kim, S. J. (2020). RPAS delivery scheduling optimization considering payload-induced battery consumption rates. *Journal of Intelligent and Robotic Systems*, 97, 471–487. <https://doi.org/10.1007/s10846-019-01034-w>
- Trotta, A., Felice, M. D., Montori, F., Chowdhury, K. R., & Bononi, L. (2018). Joint coverage, connectivity, and charging strategies for distributed UAV networks. *IEEE Transactions on Robotics*, 34(4), 883–900. <https://doi.org/10.1109/TRO.2018.2839087>
- Troudi, A., Addouche, S.-A., Dellagi, S., & Mhamedi, A. E. (2018). Sizing of the drone delivery fleet considering energy autonomy. *Sustainability*, 10, 3344. <https://doi.org/10.3390/su10093344>
- Vu, L., Vu, D. M., Hà, M. H., & Nguyen, V. (2022). The two-echelon routing problem with truck and RPASs. *International Transactions in Operational Research*, 29(5), 2968–2994. <https://doi.org/10.48550/arXiv.2004.02275>
- Wang, K., Yuan, B., Zhao, M., & Lu, Y. (2020). Cooperative route planning for the RPAS and truck in delivery services: A bi-objective optimisation approach. *The Journal of the Operational Research Society*, 71(10), 1657–1674. <https://doi.org/10.1080/01605682.2019.1621671>
- Wang, X., Yin, S., Luo, L., & Qiao, X. (2024). Research on multi-UAV task assignment based on a multi-objective, improved brainstorming optimization algorithm. *Applied Sciences*, 14, 2365. <https://doi.org/10.3390/app14062365>
- Washington, A., Clothier, R. A., & Silva, J. (2017). A review of unmanned aircraft system ground risk models. *Progress in Aerospace Sciences*, 95, 24–44.
- Wei, X., Yang, H., & Huang, W. T. (2021). A genetic-algorithm-based optimization routing for FANETs. *Frontiers in Neurorobotics*, 15, 697624. <https://doi.org/10.3389/fnbot.2021.697624>

- Wu, G., Mao, N., Luo, Q., Xu, B., Shi, J., & Suganthan, P. N. (2022). Collaborative truck-drone routing for contactless parcel delivery during the epidemic. *IEEE Transactions on Intelligent Transportation Systems*, 23, 25077–25091.
- Yadav, V. & Narasimhamurthy A. (2017). A heuristics based approach for optimizing delivery schedule of an Unmanned Aerial Vehicle (Drone) based delivery system. In *2017 ninth international conference on advances in pattern recognition (ICAPR)*, Bangalore, India, 2017 (pp. 1–6). <https://doi.org/10.1109/ICAPR.2017.8593145>.
- Yakıcı, E., & Karatas, M. (2021). Solving a multi-objective heterogeneous sensor network location problem with genetic algorithm. *Computer Networks*, 192, 108041. <https://doi.org/10.1016/j.comnet.2021.108041>
- Yang, M., Liu, G., Zhou, Z., & Wang, J. (2023). Partially observable mean field multi-agent reinforcement learning based on graph attention network for UAV swarms. *Drones*, 7, 476.
- Yu, S., Puchinger, J., & Sun, S. (2022). Van-based robot hybrid pickup and delivery routing problem. *European Journal of Operational Research*, 298(3), 894–914. <https://doi.org/10.1016/j.ejor.2021.06.009>
- Zhang, X., Chen, L., Gendreau, M., & Langevin, A. (2022). Learning-based branch-and-price algorithms for the vehicle routing problem with time windows and two-dimensional loading constraints. *INFORMS Journal on Computing*, 34(3), 1419–1436.

Publisher's Note Springer Nature remains neutral with regard to jurisdictional claims in published maps and institutional affiliations.

Authors and Affiliations

Armin Mahmoodi¹ · Seyed Mojtaba Sajadi²  · Abdellatif M. Sadeq³ · Masoud Narenji⁴ · Mehdi Eshaghi¹ · Milad Jasemi⁵

✉ Seyed Mojtaba Sajadi
s.sajadi@aston.ac.uk

Armin Mahmoodi
Arminmahmoodi@cmail.carleton.ca

Abdellatif M. Sadeq
as1004958@qu.edu.qa

Masoud Narenji
masoud.narenji@gmail.com

Mehdi Eshaghi
mehdieshaghi@cunet.carleton.ca

Milad Jasemi
mjasemiz@montevallo.edu

- ¹ Department of Aerospace Engineering, Carleton University, Ottawa, ON, Canada
- ² Operations and Information Management Department, Aston Business School, Aston University, Birmingham B4 7ET, UK
- ³ Mechanical and Industrial Engineering Department, Qatar University, Doha, Qatar
- ⁴ Department of Industrial Engineering, Iran University of Science and Technology, Tehran, Iran
- ⁵ Stephens College of Business, University of Montevallo, Montevallo, AL, USA